Nano Today 53 (2023) 102047

Contents lists available at ScienceDirect

Nano Today

journal homepage: www.elsevier.com/locate/nanotoday

Dual-switched carbon monoxide nano gas tank for auto-diagnosis and precision therapy of osteoarthritis

Xiaoting Gao [a,b], Lei Yan [a], Wei Zhang [c], Yuanliang Lv [a], Peiyan Ou [a], Ruiqiang Hang [d], Ang Gao [a], Liping Tong [a], Paul K. Chu [e], Huaiyu Wang [a,b,*]

[a] Center for Human Tissues and Organs Degeneration, Shenzhen Institute of Advanced Technology, Chinese Academy of Sciences, Shenzhen 518055, China
[b] University of Chinese Academy of Sciences, Beijing, China
[c] Technical Institute of Physics and Chemistry, Chinese Academy of Sciences, Beijing 100080, China
[d] Shanxi Key Laboratory of Biomedical Metal Materials, College of Materials Science and Engineering, Taiyuan University of Technology, Taiyuan 030024, China
[e] Department of Physics, Department of Materials Science and Engineering, And Department of Biomedical Engineering, City University of Hong Kong, Tat Chee Avenue, Kowloon, Hong Kong, China

ARTICLE INFO

Keywords:
Osteoarthritis
Carbon monoxide
Nano gas tank
Synergistic therapy
Auto-diagnosis

ABSTRACT

Carbon monoxide (CO) has great potential in the therapy of osteoarthritis (OA), but its controllable delivery *in vivo* is still an intractable problem. To optimize CO gas therapy for OA, a stable CO release platform with multi-stimulus responsiveness must be designed. Herein, we describe a local delivery system ($Fe_3(CO)_{12}$ @Croc-PEG5K) for near-infrared fluorescence (NIRF) imaging-guided photothermal treatment and CO gas synergistic therapy. As a nano gas tank, $Fe_3(CO)_{12}$ @Croc-PEG5K releases CO on-demand under near infrared (NIR) laser irradiation, scavenges free radicals and regulates the pH in the OA microenvironment, and relieves the inflammatory response of macrophages to maintain the vitality of chondrocytes. Furthermore, the pH-dependent NIRF imaging properties of $Fe_3(CO)_{12}$ @Croc-PEG5K can be exploited to determine the administration interval and auto-monitor the curative effects during the therapeutic process. Owing to these merits, the photothermal and CO gas synergistic therapy mediated by $Fe_3(CO)_{12}$ @Croc-PEG5K can be optimized to deliver outstanding therapeutic performance *in vivo*, as demonstrated by the OA rat model. Our study is the first to validate the therapeutic effect of CO against OA *in vivo*, reveals a promising strategy for precision medicine pertaining to the treatment of OA and broadens the scope of CO gas therapy.

Introduction

Osteoarthritis (OA) is a progressive and degenerative disease characterized by the degradation of cartilage, subchondral bone thickening, osteophyte formation, synovial inflammation, and ligament and meniscus injury, which is caused by the complex interactions among heredity, metabolism, biochemistry, and biomechanics [1–4]. As a kind of refractory orthopedic disorder, OA usually causes physical pain, psychological pressure, inconvenience in the daily life of patients, and social burden [5–7]. The current treatment options for OA include physiotherapy, surgical intervention, and drug therapy [8–10]. Physiotherapy is usually time-consuming and may not be effective for some patients [11–15], while surgical intervention is a costly and more risky option [16–19]. Therefore, drug therapy is the preferred OA treatment [20]. The clinical drugs for OA treatment mainly include analgesics, and non-steroidal anti-inflammatory drugs (NSAIDs) [21]. However, these first-line medicines can only provide symptomatic relief and slow down the deterioration of OA, but not completely reverse the disease progression [22–25]. In addition, there are some non-negligible problems in the clinical administration of these drugs. For example, analgesics are addictive [26], and NSAIDs may cause upper gastrointestinal complications and cardiovascular diseases [27]. Hence, it is highly desirable to develop safe and reliable therapeutic drugs based on the specific pathological characteristics of OA, and a goal of precision therapy can be achieved by on-demand administration while the therapeutic efficacy is monitored in real-time.

Among the various burgeoning medical methods, gas therapy has aroused much interest as a possible OA therapy [28,29]. Previous

* Corresponding author at: Center for Human Tissues and Organs Degeneration, Shenzhen Institute of Advanced Technology, Chinese Academy of Sciences, Shenzhen 518055, China.
E-mail address: hy.wang1@siat.ac.cn (H. Wang).

https://doi.org/10.1016/j.nantod.2023.102047
Received 3 September 2023; Received in revised form 2 October 2023; Accepted 23 October 2023

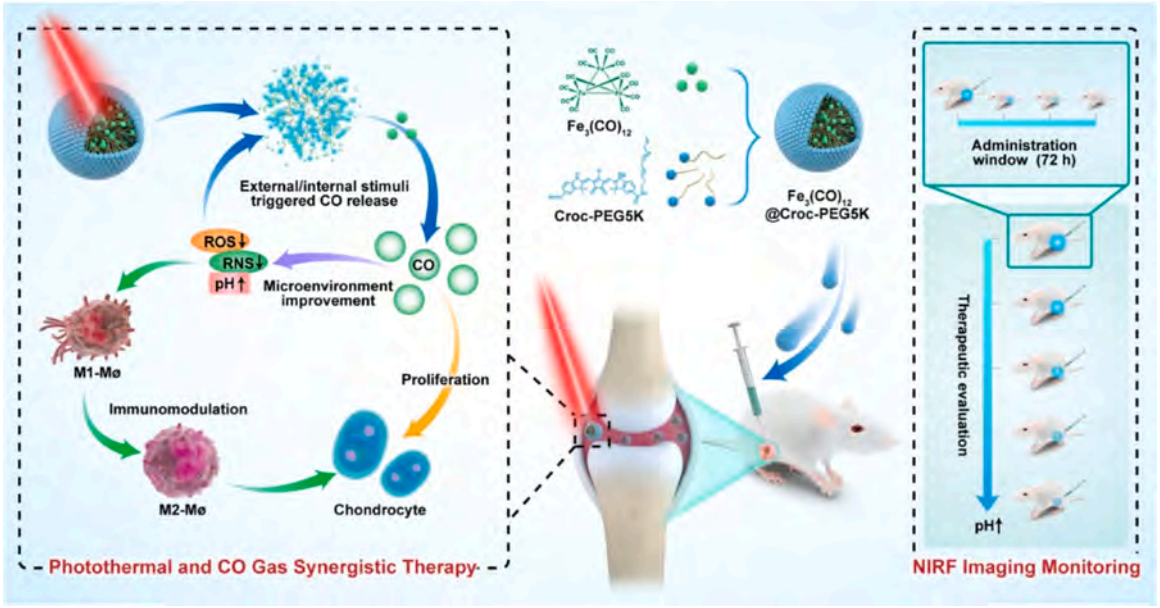

Scheme 1. Schematic illustration of $Fe_3(CO)_{12}$ @Croc-PEG5K for NIRF imaging-guided photothermal and CO gas synergistic therapy of OA.

studies reveal that a certain dose of hydrogen (H_2) can alleviate the inflammatory response of OA in the animal model [30]. Compared to H_2, carbon monoxide (CO) can provide more diverse biological effects [31], such as regulating vascular tension to promote blood circulation and reduce blood stasis [32], reducing oxidative stress to relieve inflammation [33], exerting anti-apoptotic effects to inhibit mitochondrial apoptosis [34], and promoting tissue regeneration by ameliorating the physiological microenvironment [35]. All these features are desirable for the treatment of OA which shows symptoms such as local swelling, excessive inflammation, and cartilage degradation [36–38]. It is hence reasonable to speculate that CO can be the preferred therapeutic agent for OA. However, gaseous CO is diffusible making its concentration and local delivery uncontrollable *in vivo*, probably causing invalidity and even poisoning risks [39–42]. Therefore, stable CO-releasing molecules (CORMs) and multi-functional transport vehicles must be designed for the intelligent delivery and controllable release of CO in OA treatment.

As complexes formed by transition metals (nickel, cobalt, ruthenium, vanadium, chromium, manganese, and iron) and CO, carbonyl metals are the storage tanks of CO gas and are capable of releasing CO under specific conditions such as light, heat, pH, and magnetism [43–45]. When considering the biosafety of metal metabolites, carbonyl manganese, and carbonyl iron are more suitable than others in biological applications because manganese and iron are trace elements in the human body [46–48]. In particular, $Fe_3(CO)_{12}$ has the highest gas storage capacity, making it an excellent candidate for CO storage and release [49]. Nevertheless, the poor water solubility of $Fe_3(CO)_{12}$ as well as other carbonyl metals poses a challenge in transportation *in vivo*, and a hydrophilic and biocompatible carrier that can deliver $Fe_3(CO)_{12}$ is required [50]. Furthermore, if the carrier is versatile enough to have both diagnostic and therapeutic capabilities besides good maneuverability, optimal CO gas therapy can be achieved.

Croc-PEG5K is an organic compound consisting of the croconium dye and the polyethylene glycol (PEG) polymer chain with good hydrophilic characteristics on one end and hydrophobicity on the other end [51]. The unique structure makes it an excellent candidate to envelop CORM to overcome the poor water solubility and short half-life. Moreover, Croc-PEG5K exhibits a significant photothermal effect when exposed to near-infrared (NIR) laser irradiation boding well for both photothermal physiotherapy and stimulated CO release. What is more promising, Croc-PEG5K is suitable for pH-sensitive near-infrared fluorescence (NIRF) imaging, not only for the determination of the effective time window after administration, but also for real-time auto-monitoring of the changes in the pathological microenvironment for self-evaluation. Therefore, Croc-PEG5K is a desirable delivery vehicle from many aspects.

In this study, an intelligent CO delivery system with photothermal capability, responsiveness to reactive oxide species (ROS) and reactive nitrogen species (RNS) [52], as well as the pH-dependent NIRF is designed by encapsulating $Fe_3(CO)_{12}$ into Croc-PEG5K. The core-shell nano gas tank $Fe_3(CO)_{12}$ @Croc-PEG5K can be easily formed *via* the hydrophilic and hydrophobic interactions between $Fe_3(CO)_{12}$ and Croc-PEG5K. After intra-articular injection, early release of CO from $Fe_3(CO)_{12}$ @Croc-PEG5K is triggered photothermally upon NIR laser irradiation to scavenge the overexpressed ROS/RNS and promote pH normalization. Meanwhile, ROS/RNS can serve as the internal stimuli to promote CO release under pathological conditions, achieving a virtuous cycle by ameliorating the microenvironment in the articular cavities. Controllable release of CO not only alleviates the inflammatory symptoms of macrophages to protect the damaged cartilage, but also exerts a positive effect on the proliferation of chondrocytes. Owing to the dual effects of CO gas therapy, the integrity of the cartilage can be preserved. Furthermore, NIRF imaging can be utilized to visualized the retention of $Fe_3(CO)_{12}$ @Croc-PEG5K in the articular cavities to determine the administration window, and provide real-time feedback on the therapeutic efficacy by auto-monitoring the acidity change at the lesion sites (Scheme 1). To the best of our knowledge, this is the first demonstration of the synergistic therapeutic activity of photothermal therapy and CO gas therapy for OA and integration of diagnosis and therapy by utilizing the pH-sensitive NIRF imaging capability of $Fe_3(CO)_{12}$ @Croc-PEG5K. Our study provides not only a theoretical basis for CO gas therapy on inflammatory diseases, but also guidance on how to overcome the various challenges associated with OA.

Experimental section

Materials

Dodecacarbonyltriiron (99 %, Sigma), tetrahydrofuran (THF, 99 %, Lingfeng), hemoglobin (Hb, 98 %, Aladdin), sodium dithionite (SDT, 99 %, Energy Chemical), hydrogen peroxide (30 %, Lingfeng), ethanol (99.5 %, Lingfeng), 2-phenyl-4,4,5,5-tetramethylimidazoline-1-oxyl-3-oxide (PTIO, 98 %, Energy Chemical), 1,1-diphenyl-2-picrylhydrazyl

radical (DPPH, 97 %, Energy Chemical), lipopolysaccharide (LPS, Beyotime) dulbecco's modified eagle medium (DMEM, Hyclone), penicillin/streptomycin solution (Hyclone), fetal bovine serum (FBS, Gibco), collagenase II (Sigma), phosphate buffer saline (PBS, Hyclone), trypsin-EDTA solution (Sigma), dimethyl sulfoxide (DMSO, 99 %, Energy Chemical), cell counting kit-8 (CCK-8, Beyotime), ROS assay kit (DCFH-DA, Beibo), RNS assay kit (O52, Beibo), 4,6-diamidino-2-phenylindole (DAPI, Beyotime), calcein acetoxymethyl ester (calcein-AM, Beyotime), propidium iodide (PI, Beyotime), trizol reagent (Qiagen, Germany), trichloromethane ($CDCl_3$, 99 %, Lingfeng), propan-2-ol (IPA, 99 %, Lingfeng), diethyl pyrocarbonate (DEPC, Beyotime), revertaid first strand cDNA synthesis kit (TransGen Biotech), primers (Sangon Biotech), monosodium iodoacetate (MIA, 99 %, Macklin), living chemiluminescence (CL) ROS/RNS probe (L012, Sigma), praformaldehyde (4 %, Servicebio), hematoxylin-eosin (HE, Servicebio), safranin-O fast green (Servicebio), anti-collagen type II (Servicebio), *in situ* cell death detection kit (TUNEL, Servicebio), anti-MMP-13 (Servicebio), tartrate resistant acid phosphatase (TRAP, Servicebio).

Instruments

The high-resolution liquid chromatography-mass (HRLC-MS) spectra were obtained from the HRLC-MS spectrometer (Q-Exactive, Thermo, America) and the ^1H and ^{13}C nuclear magnetic resonance (NMR) spectra were acquired on the NMR spectrometer (AVANCE III 600 MHz, Bruker, Germany). The topography, size distributions and zeta potentials of the nanoparticles were characterized by transmission electron microscopy (TEM, JEM-F200, JEOL, Japan) and dynamic light scattering (DLS, Zeta Sizer Nano ZS90, Malvern, Britain). The UV–vis–NIR and Fourier transform infrared (FT-IR) spectra were obtained on the UV–vis–NIR spectrophotometer (Cary 60, Agilent Technology, America) and Fourier transform infrared spectrophotometer (Spectrum Two, PerkinElmer, America), respectively. The photothermal experiments were conducted using an 808 nm laser (LWIRPD-808–5F, Leizhiwei, China). The viability and fluorescence micro-images of the cells were assessed on a microplate reader (Varioskan Flash, Bio Tek, America) and by high-resolution confocal microscopy (STELLARIS 5 Cryo, Leica, Germany), respectively. Gene expression of cells was measured by quantitative real-time polymerase chain reaction (qPCR) using a qTOWER3 qPCR instrument (Analytik Jena, Germany). Near-infrared fluorescence (NIRF) and micro-computed tomography (Micro-CT) imaging were performed on the animals using a living multi-mode imager (IVIS Spectrum, PerkinElmer, America) and scanner (μCT100, SCANCO Medical AG, Switzerland), respectively. The histological staining and analysis were conducted on the pathological slicer (RM2016, Leica, Germany) and optical microscopic imaging system (DS-U3, Nikon, Japan).

Preparation and characterization of $Fe_3(CO)_{12}$ @Croc-PEG5K

Croc-PEG5K was synthesized by adopting the procedures described previously [51]. Croc-PEG5K (24.0 mg, 4.3 mmol) and $Fe_3(CO)_{12}$ (12.0 mg, 23.8 mmol) were dissolved in THF (6 mL), respectively. During sonication, Croc-PEG5K and $Fe_3(CO)_{12}$ were added to ultra-pure water (50 mL) dropwise and mixed thoroughly for 30 min. Argon was injected continuously to remove THF from the water. The mixture was extruded through filter membranes (0.8, 0.45 and 0.22 μm) and concentrated in ultrafiltration centrifuge tubes (10 KD) to obtain $Fe_3(CO)_{12}$ @Croc-PEG5K. The as-prepared $Fe_3(CO)_{12}$ @Croc-PEG5K was characterized by TEM, DLS, UV–vis–NIR, FT-IR and Zeta potential.

In vitro NIR-mediated CO release of $Fe_3(CO)_{12}$ @Croc-PEG5K

The $Fe_3(CO)_{12}$ @Croc-PEG5K solution (30 μM, 1.0 mL) was irradiated with an 808 nm laser with different optical densities (0.0 ~ 1.0 W/cm^2) for 16 min to obtain the photothermal temperature curves. Considering the determination of CO release by the Hb method, the intervention of Hb and reductant on the photothermal effect was also investigated. Hb (5 μM) and SDT (1.6 mg) were added to the $Fe_3(CO)_{12}$ @Croc-PEG5K solution (30 μM, 1.0 mL) and argon was injected to purge air. The solution was irradiated with the 808 nm laser with different optical densities (0.0 ~ 1.0 W/cm^2) for 16 min to obtain the photothermal temperature curves.

In the next step, the solution was irradiated with the 808 nm laser with different optical densities (0.0 ~ 1.0 W/cm^2), and the UV–vis–NIR spectra were collected in a time-dependent manner. During this process, the absorbance values at 420 nm and 432 nm were recorded to calculate the CO release at different time points according to the Hb method [48].

$$C_{co} = C_{Hb} \quad \frac{1.333Abs_{420} - Abs_{432}}{0.8543Abs_{420} + 0.9939Abs_{432}},$$

where C_{co} and C_{Hb} are the concentrations of CO and Hb, respectively and Abs_{420} and Abs_{432} are the absorbances at 420 nm and 432 nm, respectively. To further verify the controllability of CO release by the laser, the solution was subjected to the 808 nm laser (0.6 W/cm^2) irradiation with repeating "on-off" states to determine the CO release at different time points.

In vitro H2O2-mediated CO release of $Fe_3(CO)_{12}$ @Croc-PEG5K

Different concentrations of H_2O_2 (0.0 ~ 5.0 μM) were added to the solution and the UV–vis–NIR spectra were collected in a time-dependent manner. The absorbances at 420 nm and 432 nm were recorded to calculate the CO release at different time points according to the aforementioned Hb method.

In vitro ROS/RNS scavenging capacity of $Fe_3(CO)_{12}$ @Croc-PEG5K

$Fe_3(CO)_{12}$ @Croc-PEG5K (0 ~ 25 μM) was added to PTIO in the PBS solution (2.5 mM, 2 mL) and irradiated with the 808 nm laser with different optical densities (0.0 ~ 1.0 W/cm^2) for 10 min followed by measuring the absorbance at 557 nm. Similarly, $Fe_3(CO)_{12}$ @Croc-PEG5K (0 ~ 15 μM) was added to the DPPH in ethanol (2.0 mM, 2 mL) and irradiated with the 808 nm laser with different optical densities (0.0 ~ 1.0 W/cm^2) for 10 min prior to measuring the absorbance at 517 nm. The inhibition rates were calculated by the following formula [53]:

$$\text{Inhibition}(\%) = \left(\frac{A_0 - A_i - A_j}{A_0}\right) * 100\%,$$

where A_0 is the absorbance of PTIO/DPPH at 557/517 nm, A_i stands for the absorbance of the solution of PTIO/DPPH and $Fe_3(CO)_{12}$ @Croc-PEG5K at 557/517 nm, and A_j is the absorbance of $Fe_3(CO)_{12}$ @Croc-PEG5K at 557/517 nm.

Cell culture

The murine-derived macrophages (RAW264.7) were purchased from the National Collection of Authenticated Cell Cultures (Shanghai, China). The chondrocytes were extracted from the cartilage tissue of one-week-old C57BL/6J lactating mice (Vital River Laboratory, Jiaxing, Zhejiang) according to a previous study [54]. Both the RAW264.7 cells and chondrocytes were cultured in DMEM supplemented with 10 % (v/v) FBS in a humidified incubator of 5 % CO_2.

In vitro biocompatibility of $Fe_3(CO)_{12}$ @Croc-PEG5K

Both the RAW264.7 cells and chondrocytes were seeded on 96-well plates at a density of 5×10^3 cells/well and cultured at 37 ℃ for 24 h. In some groups, the culture medium was subsequently replaced with the fresh culture medium containing LPS (1 μg/mL) for another 24 h and washed with the PBS buffer thereafter. Subsequently, Croc-PEG5K and $Fe_3(CO)_{12}$ @Croc-PEG5K (0 ~ 140 μM) dissolved in the culture medium

were incubated with the cells for 24 h and replaced with fresh culture medium for 24 h after washing with PBS. Finally, the treated cells were incubated with serum-free DMEM containing CCK-8 (10 %) for 1.5 h and the absorbance at 450 nm was measured according to the standard procedure of the CCK-8 assay.

In live/dead staining, 1×10^5 RAW264.7 cells and chondrocytes were seeded on the bottom dishes (20 mm) and cultured at 37 ℃ for 24 h. In some groups, the culture medium was replaced with the fresh culture medium containing LPS (1 μg/mL) for another 24 h and washed with the PBS buffer thereafter. Subsequently, Croc-PEG5K and $Fe_3(CO)_{12}$ @Croc-PEG5K (50 μM) dissolved in the culture medium were incubated with the cells for 24 h, and then replaced with the fresh culture medium for 24 h after PBS washing. Finally, the treated cells were co-stained with calcein-AM and PI for 20 min and washed with the PBS buffer prior to fluorescence imaging.

Cellular CO release of $Fe_3(CO)_{12}$ @Croc-PEG5K in RAW264.7 cells

1×10^5 RAW264.7 cells were seeded on the bottom dishes (20 mm) and cultured at 37 ℃ for 24 h. In some groups, the culture medium was replaced with the fresh culture medium containing LPS (1 μg/mL) for another 24 h and washed with the PBS buffer thereafter. The cells were then co-stained with DAPI for 10 min and DCFH-DA/O52 for 20 min and washed with the PBS buffer prior to fluorescence imaging.

CO probe (COP) was synthesized according to a previous study [55], and characterized by HRLC-MS as well as ^1H and ^{13}C NMR. 1×10^5 RAW264.7 cells were seeded on the bottom dishes and cultured at 37 ℃ for 24 h. In some groups, the culture medium was replaced with the fresh culture medium containing LPS (1 μg/mL) for another 24 h and washed with the PBS buffer thereafter. COP (25 μM) dissolved in the culture medium was incubated with the cells for 3 h and washed with the PBS buffer. Afterwards, $Fe_3(CO)_{12}$ @Croc-PEG5K (50 μM) dissolved in DMEM was incubated with the cells for 8 h and irradiated with the 808 nm laser (1.0 W/cm^2) for 5 min. The cell culture continued for another 16 h and the cells were washed with the PBS buffer. Finally, the treated cells were stained with DAPI for 10 min and washed with the PBS buffer prior to fluorescence imaging.

Immunomodulatory effect of $Fe_3(CO)_{12}$ @Croc-PEG5K

The RAW264.7 cells were seeded on 24-well plates at a density of 2×10^4 cells/well and cultured at 37 ℃ for 24 h. In some groups, the culture medium was replaced with the fresh culture medium containing LPS (1 μg/mL) for another 24 h and washed with the PBS buffer thereafter. $Fe_3(CO)_{12}$ @Croc-PEG5K (25 and 50 μM) dissolved in DMEM was incubated with the cells for 8 h and irradiated with the 808 nm laser (1.0 W/cm^2) for 5 min. The cell culture continued for another 16 h and the cells were washed with the PBS buffer. The treated cells were cultured in the fresh culture medium for 24 h and the medium in each group was harvested. Finally, RNA was extracted from the cells by trizol, reversely transcribed into cDNA, and analyzed for the gene expressions of L-1β, IL-6, TNF-α, iNOS, IL-4, CD206, TGF-β2, and IGF-1 by qPCR.

The medium harvested from each group was mixed with the fresh culture medium at a ratio of 1:1 for the preparation of conditioned medium. Chondrocytes were seeded on 24-well plates at a density of 2×10^4 cells/well and cultured in the culture medium at 37 ℃ for 24 h. The medium was replaced with the conditioned medium in each group every 16 h and cultured for 48 h. Finally, RNA was extracted from the cells by trizol, reversely transcribed into cDNA, and analyzed for the gene expressions of Col2a1, Acan, Caspase3, and Bax by qPCR. The gene primers used in the qPCR experiments are listed in Table S1.

High-throughput RNA sequencing analysis

The RAW264.7 cells were seeded on 24-well plates at a density of 2×10^4 cells/well and cultured at 37 ℃ for 24 h. Subsequently, the culture medium was replaced with the fresh culture medium containing LPS (1 μg/mL) for another 24 h and washed with the PBS buffer thereafter. Half of the LPS-induced cells underwent 24 h of routine culture as a Control group. In the Therapy Group, the LPS-induced cells were incubated with $Fe_3(CO)_{12}$ @Croc-PEG5K (50 μM) in DMEM for 8 h, irradiated by the 808 nm laser (1.0 W/cm^2) for 5 min, and the cell culture continued for another 16 h. Finally, the medium was collected and the cells were harvested for high-throughput sequencing analysis with the technical supports from Beijing Genomics Institute (China).

The medium harvested from each group was mixed with the fresh culture medium at a ratio of 1:1 for the preparation of conditioned medium. Chondrocytes were seeded on 24-well plates at a density of 2×104 cells/well and cultured in the culture medium at 37 ℃ for 24 h. Subsequently, the medium was replaced with the conditioned medium of each group every 16 h and cultured for another 48 h. Finally, the cells were harvested for high-throughput sequencing analysis with the technical supports from Beijing Genomics Institute (China).

MIA-induced OA rats

The Sprague-Dawley (SD) rats were purchased from Vital River Laboratory (Jiaxing, Zhejiang) and all the animal experiments and protocols were approved by the Ethics Committee for Animal Research, Shenzhen Institute of Advanced Technology, Chinese Academy of Sciences. MIA was used to induce the OA condition in the experimental rats, because it could inhibit the metabolism of chondrocytes, causing chondrocyte apoptosis and extracellular matrix degradation accompanied by inflammatory response and joint pain. The SD rats were anesthetized by intraperitoneal injection of 2 % pentobarbital (2 mL/kg) and the knees were shaved and disinfected using medical iodophor. The knees were flexed at 45° and articular cavity puncturing was performed from the lateral side of the inferior ligament of the patella. The needle returned by 2 mm after reaching the femoral condyle and then MIA (20 mg/mL, 100 μL) or saline (0.9 %, 100 μL) was injected for the establishment of the OA rats or normal rats. After 48 h, different interventions were involved.

Retention in the articular cavity and biodistribution of $Fe_3(CO)_{12}$ @Croc-PEG5K

Three groups of OA rats were intra-articularly injected with saline (0.9 %, 50 μL) and $Fe_3(CO)_{12}$ @Croc-PEG5K (150 and 300 μM, 50 μL), respectively. The NIRF images were obtained at 0, 24, 48, and 72 h post-injection and the corresponding intensity was determined. At 72 h after intra-articular injection, all rats were dissected to obtain the main organs separately and determined by NIRF imaging.

In vivo microenvironment monitoring and ROS/RNS scavenging capacity of $Fe_3(CO)_{12}$ @Croc-PEG5K

Two groups of normal rats and two groups of OA rats were intra-articularly injected with saline (0.9 %, 50 μL) after 2, 5, 8, and 11 days. After 14 days, all the rats were injected with $Fe_3(CO)_{12}$ @Croc-PEG5K (150 and 300 μM, 50 μL) and subjected to NIRF imaging. At the same time, two groups of OA rats were injected with $Fe_3(CO)_{12}$ @Croc-PEG5K (150 and 300 μM, 50 μL) after 2, 5, 8, 11, and 14 days. NIRF imaging was performed after each injection and the corresponding intensity was recorded.

One group of normal rats and one group of OA rats were intra-articularly injected with saline (0.9%, 50 μL) after 2, 5, 8, 11, and 14 days, and two groups of OA rats were injected with $Fe_3(CO)_{12}$ @Croc-PEG5K (150 and 300 μM, 50 μL) after 2, 5, 8, 11, and 14 days. After 17 days, all the rats were injected with ROS/RNS-responsive CL probe L012 for imaging and the corresponding CL intensity was recorded.

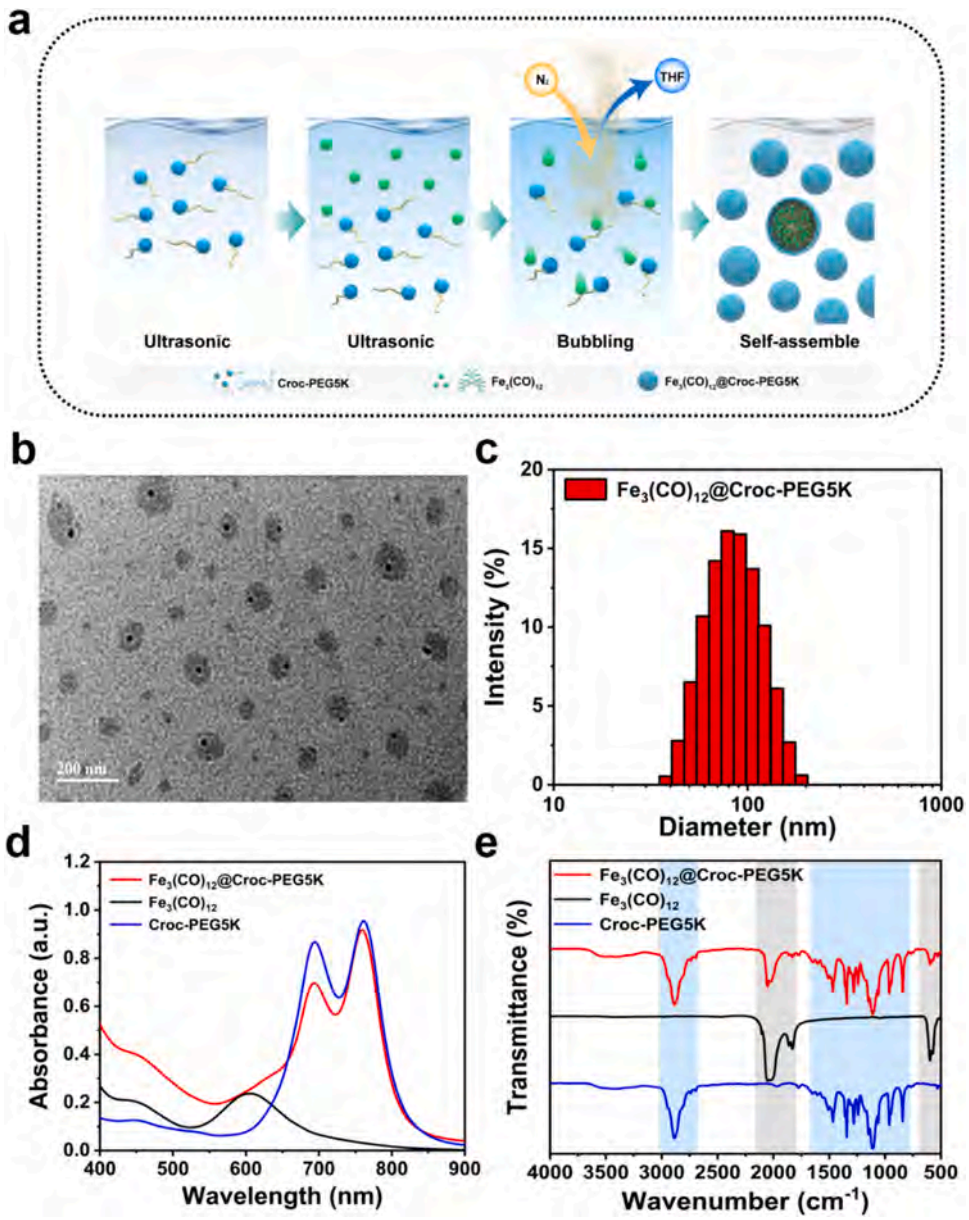

Fig. 1. Preparation and characterization of $Fe_3(CO)_{12}$ @Croc-PEG5K. (a) Schematic illustration of the fabrication of $Fe_3(CO)_{12}$ @Croc-PEG5K; (b) TEM image (Scale bar = 200 nm) and (c) DLS size distribution of $Fe_3(CO)_{12}$ @Croc-PEG5K; (d) UV–vis–NIR absorption and (e) FT-IR spectra of $Fe_3(CO)_{12}$ @Croc-PEG5K, $Fe_3(CO)_{12}$ and Croc-PEG5K.

In vivo photothermal effect of $Fe_3(CO)_{12}$ @Croc-PEG5K

Three groups of OA rats were intra-articularly injected with saline (0.9 %, 50 μL) and $Fe_3(CO)_{12}$ @Croc-PEG5K (150 and 300 μM, 50 μL), respectively. Afterwards, all the rats were exposed to the 808 nm laser (1.0 W/cm^2) for 10 min and the corresponding temperature and thermal images were collected at different time points.

In vivo therapeutic efficacy of $Fe_3(CO)_{12}$ @Croc-PEG5K

One group of normal rats and one group of OA rats were intra-articularly injected with saline (0.9 %, 50 μL) after 2, 5, 8, 11, and 14 days. Four groups of OA rats were injected with $Fe_3(CO)_{12}$ @Croc-PEG5K (150 and 300 μM, 50 μL) after 2, 5, 8, 11, and 14 days, and half of them were exposed to the 808 nm laser (1.0 W/cm^2) for 10 min after each injection. After 17 days, blood was collected from the different groups of rats for biochemical and blood routine assessment. Finally, all the rats were dissected to extract the main organs (heart, liver, spleen, lung, and kidney) for histological analysis. The knee joints of rats after different treatments were harvested for micro-CT imaging as well as histological and immunohistochemical staining to evaluate the therapeutic efficacy.

Results and discussion

Preparation and characterization of $Fe_3(CO)_{12}$ @Croc-PEG5K

$Fe_3(CO)_{12}$ @Croc-PEG5K is synthesized by the hydrophilic-hydrophobic interactions as shown in Fig. 1a. The amphiphilic Croc-PEG5K is used to encapsulate the hydrophobic $Fe_3(CO)_{12}$ to produce $Fe_3(CO)_{12}$ @Croc-PEG5K with a uniform morphology and an average size of 100 nm (Fig. 1b, c). Formation of $Fe_3(CO)_{12}$ @Croc-PEG5K is confirmed by UV–vis–NIR spectrophotometry, FT-IR spectroscopy and the measurement of Zeta potential (Fig. 1d, e and Fig. S1). The as-

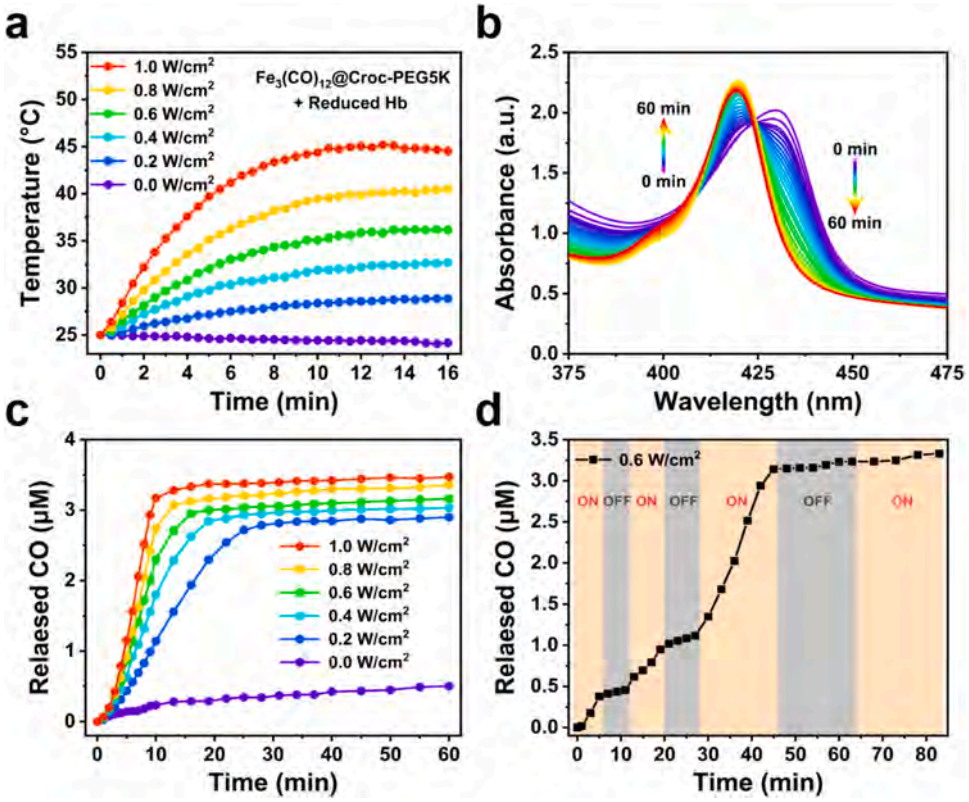

Fig. 2. NIR laser-mediated CO release of $Fe_3(CO)_{12}$ @Croc-PEG5K *in vitro* [NIR laser parameter: 808 nm; Solution: $Fe_3(CO)_{12}$ @Croc-PEG5K (30 μM) and reduced Hb (5 μM) in PBS buffer (pH 6.8)]. (a) Temperature evaluation upon NIR laser irradiation with different optical densities (0.0 ~ 1.0 W/cm^2); (b) UV–vis–NIR absorption spectra under NIR laser irradiation (0.6 W/cm^2) at different time points (0 ~ 60 min); (c) Time-dependent CO release under NIR laser illumination with different optical densities (0.0 ~ 1.0 W/cm^2); (d) CO release in repeated NIR laser "on-off" states (0.6 W/cm^2).

prepared $Fe_3(CO)_{12}$ @Croc-PEG5K can be dispersed in various media (Fig. S2), which provides good storage stability without noticeable aggregation in 72 h (Fig. S3). Even after 4 centrifugation-ultrasonic-resuspension cycles, no dye dissociation and $Fe_3(CO)_{12}$ leakage is observed, suggesting strong binding between Croc-PEG5K and $Fe_3(CO)_{12}$ (Fig. S4). The relationship between the Croc-PEG5K concentration and absorbance at 760 nm (Abs_{760}) is established to quantify $Fe_3(CO)_{12}$ @Croc-PEG5K in the following study (Fig. S5).

In vitro CO release of $Fe_3(CO)_{12}$ @Croc-PEG5K

CO release from $Fe_3(CO)_{12}$ @Croc-PEG5K is investigated *in vitro* by the reduced Hb method [48]. Compared to $Fe_3(CO)_{12}$ @Croc-PEG5K only, the solution of $Fe_3(CO)_{12}$ @Croc-PEG5K, Hb, and SDT (a reductive agent) exhibits weaker photothermal effects under the same 808 nm laser irradiation (Fig. 2a and Fig. S6), probably due to the presence of protein macromolecules and the reducibility of SDT. The reduced Hb, which shows an absorption peak at 432 nm, reacts with released CO to form carboxyhemoglobin (COHb), and the absorption peak blue-shifts to 420 nm (Fig. 2b). Hence, the amount of CO release can be monitored, and the result indicates that more intense NIR laser irradiation will lead to more CO release within a period of time (Fig. 2c). To verify the controllability, CO release from $Fe_3(CO)_{12}$ @Croc-PEG5K is investigated during repetitive NIR laser "on-off" manipulation. When the laser is on, CO release is initiated due to the higher temperature. When it is off, CO release slows down since the temperature decreases (Fig. 2d). $Fe_3(CO)_{12}$ @Croc-PEG5K is further analyzed *in vitro* to determine its capacity to scavenge free radicals under different NIR irradiation conditions. Fig. S7 shows that $Fe_3(CO)_{12}$ @Croc-PEG5K can scavenge 98% of PTIO (commercial ROS) and DPPH (commercial RNS) when the NIR laser power is 1.0 W/cm^2. Therefore, $Fe_3(CO)_{12}$ @Croc-PEG5K has great potential in ameliorating the pathological microenvironment of OA with free radical overexpression. Free radicals such as H_2O_2 can also trigger the release of CO. As shown in Fig. S8, the higher the concentration of H_2O_2, the faster the CO release rate from $Fe_3(CO)_{12}$ @Croc-PEG5K. Our results show that CO release from $Fe_3(CO)_{12}$ @Croc-PEG5K can be mediated by external NIR irradiation as well as free radicals in the pathological microenvironment. This controllable property is desirable for maintaining the CO concentration within the therapeutic window and minimizing possible side effects.

In vitro biocompatibility of $Fe_3(CO)_{12}$ @Croc-PEG5K

Next, the biocompatibility of $Fe_3(CO)_{12}$ @Croc-PEG5K to Raw264.7 cells (a kind of monocyte macrophages) and chondrocytes is assessed. As shown in Fig. 3a, $Fe_3(CO)_{12}$ @Croc-PEG5K provides a better biocompatibility to normal Raw264.7 cells than Croc-PEG5K and the safe concentration is as high as 120 μM. However, under LPS stimulation, the viability of the Raw264.7 cells after the Croc-PEG5K treatment is slightly higher, especially when the concentration of Croc-PEG5K is 10 ~ 80 μM, probably because CO release from $Fe_3(CO)_{12}$ @Croc-PEG5K is faster under inflammatory conditions. Furthermore, $Fe_3(CO)_{12}$ @Croc-PEG5K at high concentrations significantly promotes the proliferation of LPS-induced chondrocytes as manifested by the higher cell viability (Fig. 3b), indicating that CO released from $Fe_3(CO)_{12}$ @Croc-PEG5K produces anti-apoptotic effects on chondrocytes in a dose-dependent manner. Live/dead staining is also performed on the cells after different treatments. As shown in Fig. 3c, although there are more dead Raw264.7 cells exhibiting red fluorescence after LPS stimulation, the viable cells showing green fluorescence are still dominant with insignificant difference among the 3 groups. As for chondrocytes, the percentage of dead cells do not increase after LPS stimulation, and a higher

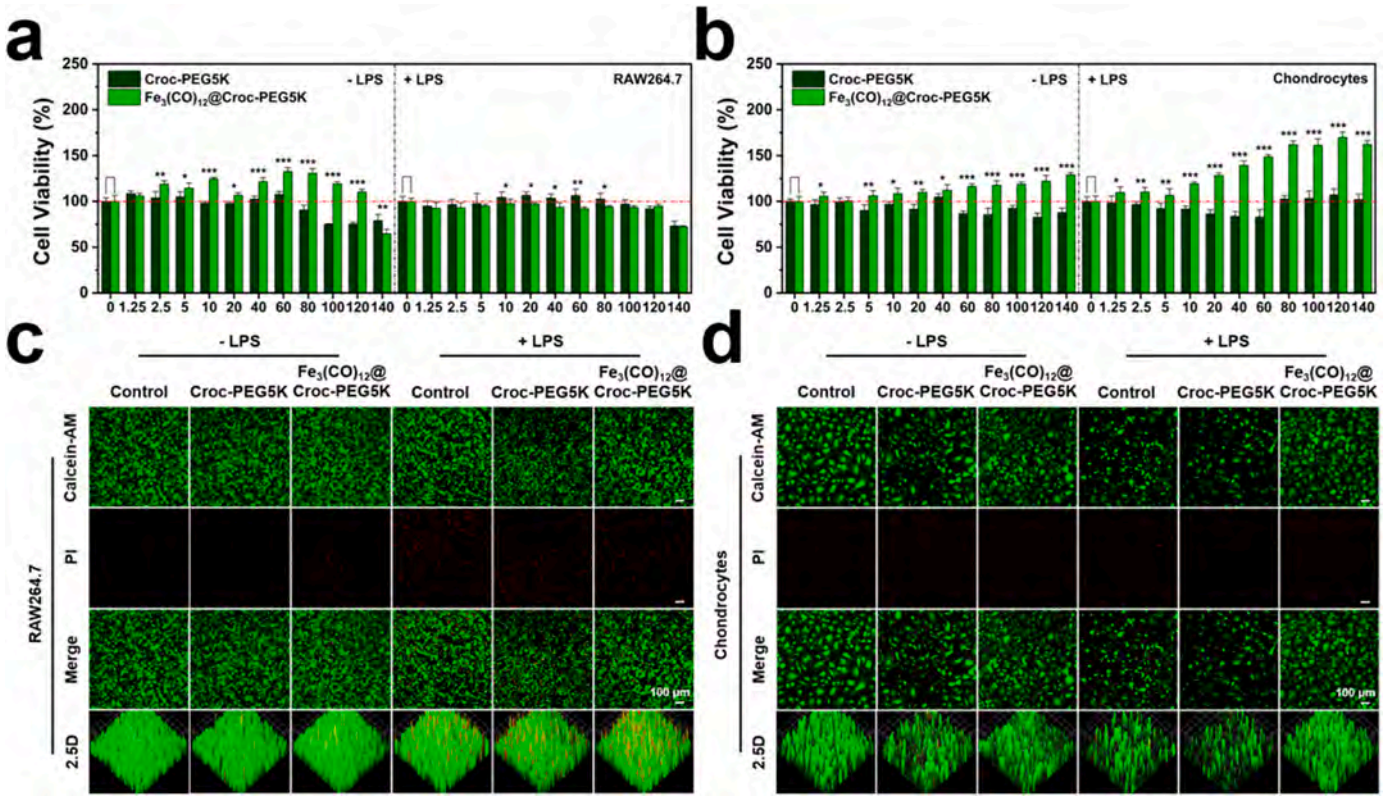

Fig. 3. *In vitro* biocompatibility of $Fe_3(CO)_{12}$ @Croc-PEG5K. Effects of Croc-PEG5K and $Fe_3(CO)_{12}$ @Croc-PEG5K (0 ~ 140 μM) on the viability of (a) Raw264.7 cells and (b) Chondrocytes with or without LPS stimulation; Live/dead staining of (c) Raw264.7 cells and (d) chondrocytes with or without LPS stimulation after the treatment of Croc-PEG5K and $Fe_3(CO)_{12}$ @Croc-PEG5K (50 μM). Scale bar = 100 μm.

density of live cells is observed from the $Fe_3(CO)_{12}$ @Croc-PEG5K groups (Fig. 3d). These findings corroborate the results of cell viability assay.

Cellular CO release of $Fe_3(CO)_{12}$ @Croc-PEG5K

In order to monitor intracellular CO release from $Fe_3(CO)_{12}$ @Croc-PEG5K, a CO probe (COP) is synthesized, characterized (Fig. S9-11), and utilized in our study [55]. After culturing Raw264.7 cells with COP, some groups are treated by $Fe_3(CO)_{12}$ @Croc-PEG5K (50 μM) with or without NIR irradiation (1.0 W/cm^2, 5 min). As shown in Fig. 4, the $Fe_3(CO)_{12}$ @Croc-PEG5K with intrinsic NIRF signal can be endocytosed by macrophages. Meanwhile, the fluorescent intensity of COP, which is an indicator of the intracellular CO level, is enhanced by NIR laser irradiation. In addition to the NIR laser-triggered CO release, LPS stimulation induces M1 polarization of RAW264.7 cells with overexpressed ROS/RNS (Fig. S12), which then reacts with $Fe_3(CO)_{12}$ @Croc-PEG5K to generate CO. Therefore, after the same $Fe_3(CO)_{12}$ @Croc-PEG5K treatment, intracellular COP fluorescence from the LPS-induced macrophages is more intense than that without LPS stimulation. It is worth mentioning that the photothermal effect of $Fe_3(CO)_{12}$ @Croc-PEG5K under this condition is moderate (< 35 °C), which does not pose a negative effect on the viability of cultured cells (Fig. S13).

Immunomodulatory effect of $Fe_3(CO)_{12}$ @Croc-PEG5K

To verify the immunomodulatory effect, the LPS-induced RAW264.7 cells undergo $Fe_3(CO)_{12}$ @Croc-PEG5K treatment and NIR irradiation following the procedure shown in Fig. 5a. The results show that $Fe_3(CO)_{12}$ @Croc-PEG5K, especially with the aid of NIR irradiation (1.0 W/cm^2, 5 min), down-regulates the expression of M1-related genes (IL-1β, IL-6, TNF-α, and iNOS) in the LPS-induced macrophages at M1 phenotype (Fig. 5b-e). Meanwhile, the anti-inflammatory genes (IL-4 and CD206) and pro-chondrogenic genes (TGF-β2 and IGF-1) of the LPS-induced macrophages are up-regulated in the presence of $Fe_3(CO)_{12}$ @Croc-PEG5K, thereby creating the desirable local inflammation-relieved microenvironment for cartilage protection (Fig. 5f-i). With regard to the macrophages-chondrocytes cascade reaction, conditioned medium (CM) is prepared after culturing the LPS-induced macrophages with $Fe_3(CO)_{12}$ @Croc-PEG5K and used for the cultivation of chondrocytes (Fig. 5a). It is clear that the anti-inflammatory effect of $Fe_3(CO)_{12}$ @Croc-PEG5K benefits the vitality maintenance of chondrocytes, as reflected by up-regulation of the chondrogenesis-related genes (Col2a1 and Acan) and down-regulation of the apoptosis-related genes (Caspase3 and Bax) after conditioned culturing (Fig. 5j-m).

Immunoregulatory mechanism of $Fe_3(CO)_{12}$ @Croc-PEG5K

To further explore the underlying mechanism of $Fe_3(CO)_{12}$ @Croc-PEG5K about immunoregulation, high-throughput sequencing analysis is performed in our study. In particular, the LPS-induced RAW264.7 cells undergoing routine culture are considered as a Control group, and those in the Therapy group are subjected to $Fe_3(CO)_{12}$ @Croc-PEG5K treatment together with NIR irradiation (5 min, 1.0 W/cm^2). Both groups of cells are collected and analyzed by RNA sequencing. As the volcano plot of differentially expressed genes (DEGs) shown in Fig. 6a, there are a total of 1937 down-regulated genes and 1718 up-regulated genes between the Therapy group and Control group. Pearson correlation coefficient analysis (Fig. S14a) and principal component analysis (Fig. S14b) demonstrate that the samples in each group provide high correlation of gene expression and good reproducibility. Among the DEGs with significant difference (Fig. 6b), those related to macrophage phenotypes and inflammatory cytokine expressions are highlighted (Fig. 6c). It is remarkable that the pro-inflammatory cytokines of macrophages such as

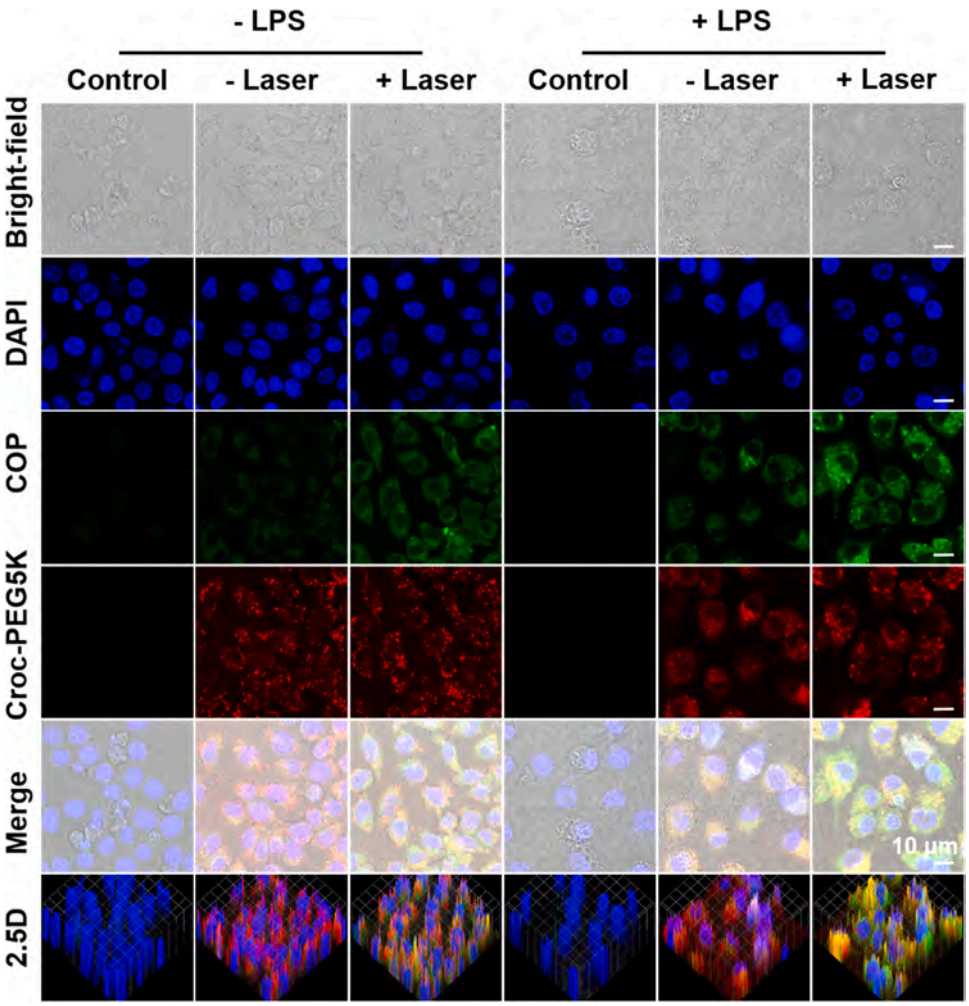

Fig. 4. Fluorescent images of Raw264.7 cells after different treatments (Blue channel: λex: 405 nm, λem: 437 nm; Green channel: λex: 458 nm, λem: 550; Red channel: λex: 633 nm, λem: 694 nm; Scale bar = 10 μm).

CD86, L-1α, IL-1β and IL-6 are down-regulated in the Therapy group, whereas the pro-chondrogenic and anti-apoptotic markers including IGF-1, IGF-2R and Bcl2 are up-regulated, which corroborate the aforementioned results shown in Fig. 5. Gene Ontology (GO) enrichment is also performed to explore the difference in biological process, cellular component and molecular function between the two groups (Fig. S15a). As shown in Fig. 6d, the immune response (red wireframes), stimulus induction (blue wireframes) and oxidative stress (green wireframes) are in top 30 of GO enrichment. Furthermore, to unveil the potential signaling pathways, the sequencing data are analyzed by Kyoto Encyclopedia of Genes and Genomes (KEGG) enrichment (Fig. S15b). Fig. 6e shows that the inflammatory and immune-related signaling pathways such as HIF-1 signaling pathway, IL-17 signaling pathway, chemokine signaling pathway, and TNF signaling pathway (red wireframes) are significantly enriched. Consistent with the results of GO and KEGG enrichment, gene set enrichment analysis (GSEA) reveals that the cellular response to hypoxia and the HIF-1 signaling pathway (regulation of oxygen homeostasis) are significantly down-regulated in the Therapy group (Fig. 6f, g). In addition, the key inflammatory pathways (TNF signaling pathway, IL-17 signaling pathway, NF-kappa B signaling pathway, and chemokine signaling pathway) as well as the cascade pathways (MARK signaling pathway, JAK-STAT signaling pathway, and NOD-like receptor signaling pathway) are negatively correlated with the therapy (Fig. 6h-k and Fig. S16). All these results suggest that the $Fe_3(CO)_{12}$ @Croc-PEG5K treatment combined with NIR irradiation can exert desirable immunoregulatory effects by alleviating oxidative stress and inhibiting inflammatory response of macrophages *via* multiple signaling pathways.

To investigate the mechanism of macrophages-chondrocytes cascade reaction, high-throughput sequencing analysis is also performed on chondrocytes after conditioned culture. The volcano plot shows that there are a total of 275 down-regulated genes and 915 up-regulated genes (Fig. 7a). The expression heat map of DEGs with significant difference is drawn (Fig. 7b), and genes related to inflammation (Mycbp2, Adam10, and IGF 2r), structural integrity (Adamts5, BMP2, Prg4, Col2α1, and Col2α1) and apoptosis (Trp53bp2, Bcl2l11, Bcl6, Mr1, and Sirt1) (Fig. 7c) are selected. GO classification in biological process, cellular component and molecular function (Fig. S17a), and KEGG pathway classification in cellular processes, environmental information processing, genetic information processing, human diseases, metabolism, and organismal systems (Fig. S17b) are counted. Among these omics information, the inflammation (red wireframes), matrix integrity (blue wireframes), and senescence and apoptosis (greed wireframes) are emphasized in top 30 of GO and KEGG enrichment (Fig. 7d, e). To further confirm the overall expression trend of these pathways (activated or inhibited), GSEA is analyzed. It is clear that PPAR signaling pathway (anti-inflammatory pathway) is up-regulated (Fig. 7f), hedgehog signaling pathway (promoting cartilage degeneration) and calcium signaling pathway (regulation of cartilage growth) both change to cartilage retention (Fig. 7g, h), and senescence and apoptosis-related pathways are all inhibited (Fig. 7i-k). All these results prove that $Fe_3(CO)_{12}$ @Croc-PEG5K can not only directly promote the

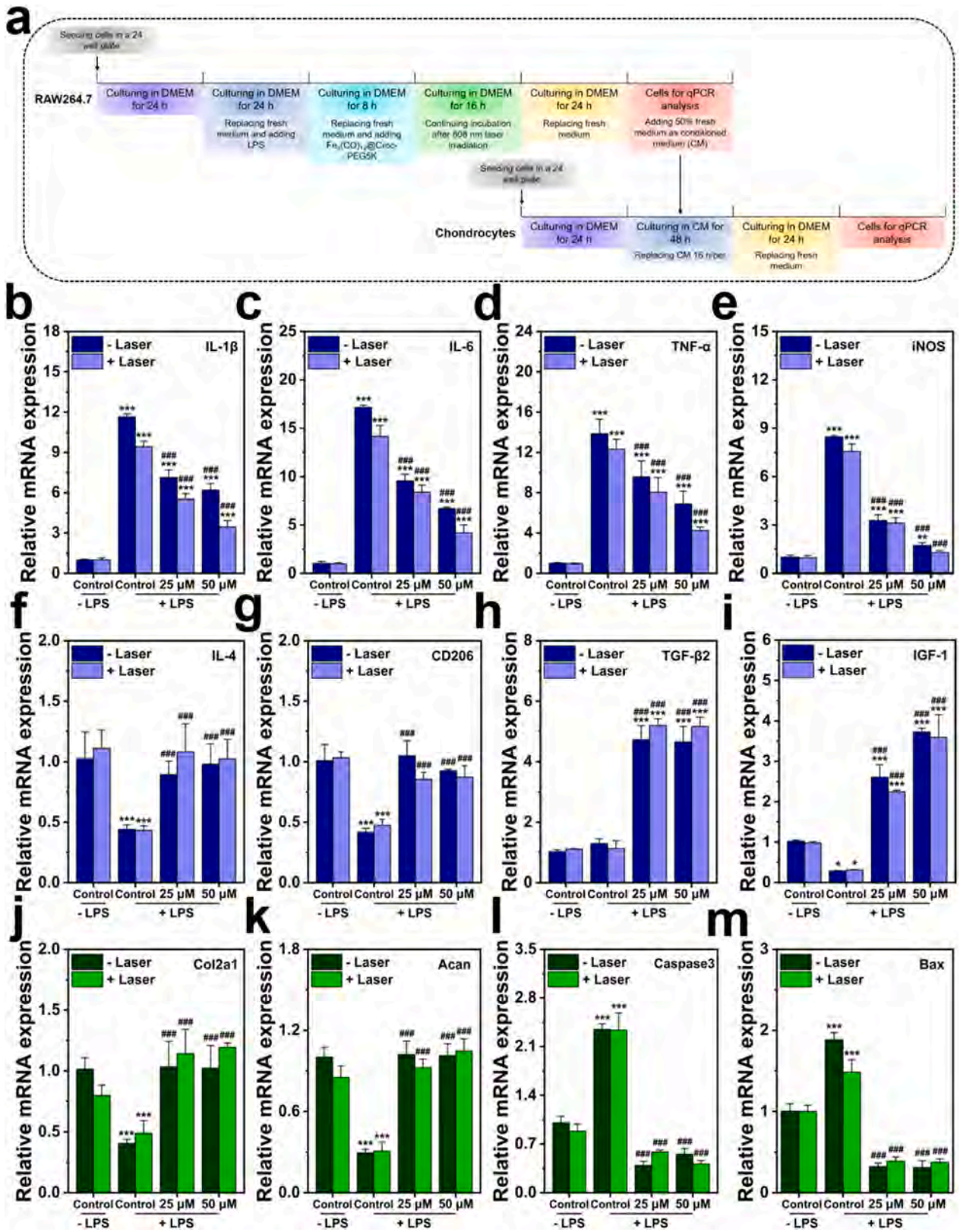

Fig. 5. Regulatory effects of $Fe_3(CO)_{12}$ @Croc-PEG5K on macrophages and macrophages-chondrocytes cascade reaction. (a) Schematic diagram of the experimental procedure; Expression levels of (b-e) M1-related genes (IL-1β, IL-6, TNF-α, and iNOS) and (f-i) M2-related genes (IL-4, CD206, TGF-β2, and IGF-1) in Raw264.7 cells after different treatments; Expression levels of (j-k) chondrogenesis-related genes (Col2a1 and Acan) and (l-m) apoptosis-related genes (Caspase3 and Bax) in chondrocytes after conditioned culture. $^{*}P < 0.05$, $^{**}P < 0.01$, $^{***}P < 0.001$, compared to the control group without LPS stimulation and laser irradiation, $^{\#}P < 0.05$, $^{\#\#}P < 0.01$, $^{\#\#\#}P < 0.001$, compared to the control group with LPS stimulation but without laser irradiation.

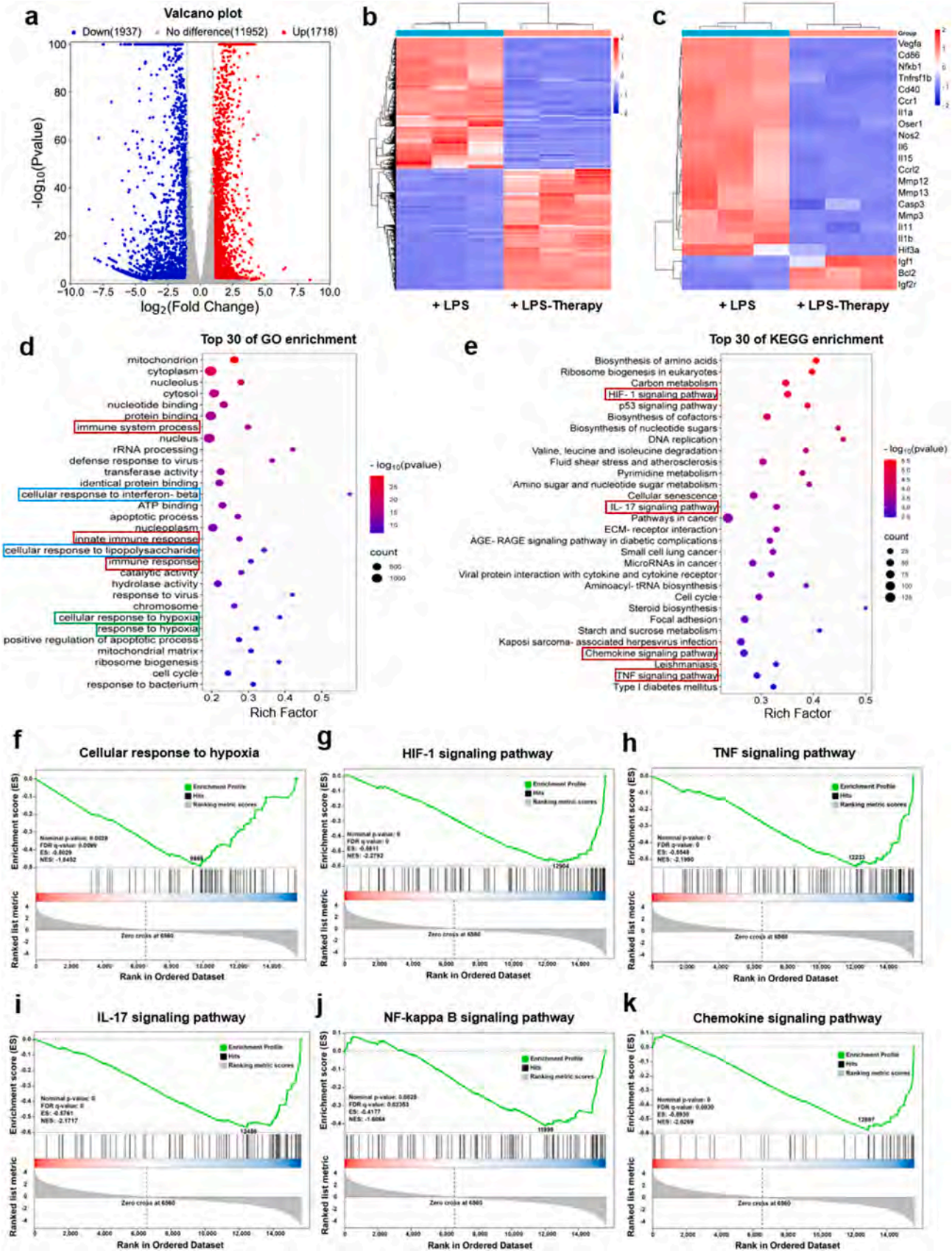

Fig. 6. High-throughput sequencing analysis of $Fe_3(CO)_{12}$ @Croc-PEG5K on macrophages. (a) Volcano plot analysis; (b) Gene heat map analysis; (c) Gene heat map of macrophage phenotype and inflammatory cytokines expression; The top 30 of (d) GO and (e) KEGG enrichment of gene expression profiles; GSEA analysis of (f) cellular response to hypoxia, (g) HIF-1 signaling pathway, (h) TNF signaling pathway, (i) IL-17 signaling pathway, (j) NF-kappa B signaling pathway, and (k) chemokine signaling pathway.

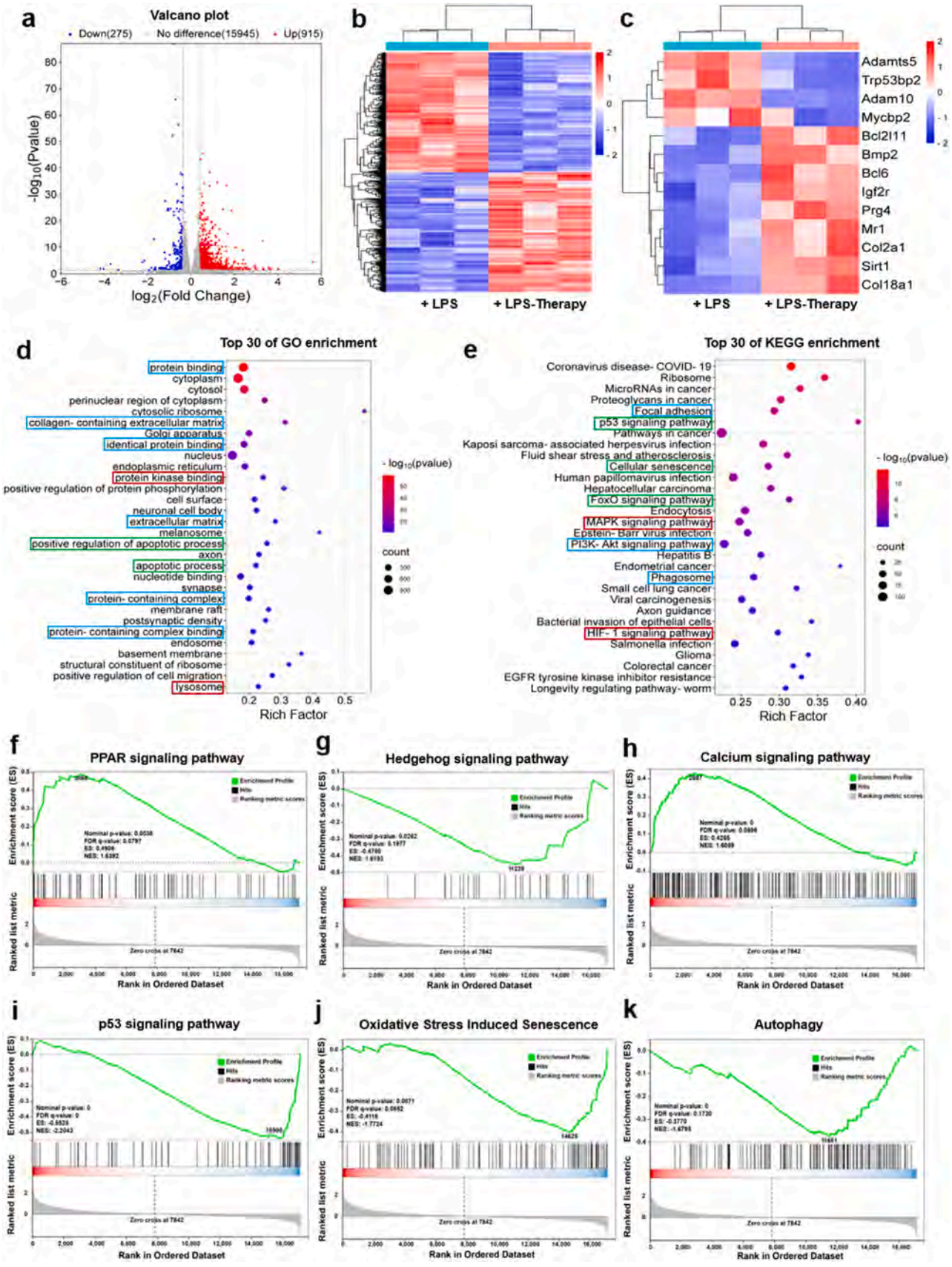

Fig. 7. High-throughput sequencing analysis of chondrocytes after conditioned culture. (a) Volcano plot analysis; (b) Gene heat map analysis; (c) Gene heat map of macrophage phenotype and inflammatory cytokines expression; The top 30 of (d) GO and (e) KEGG enrichment of gene expression profiles; GSEA analysis of (f) PPAR signaling pathway, (g) Hedgehog signaling pathway, (h) Calcium signaling pathway, (i) p53 signaling pathway, (j) Oxidative stress induced senescence, and (k) Autophagy.

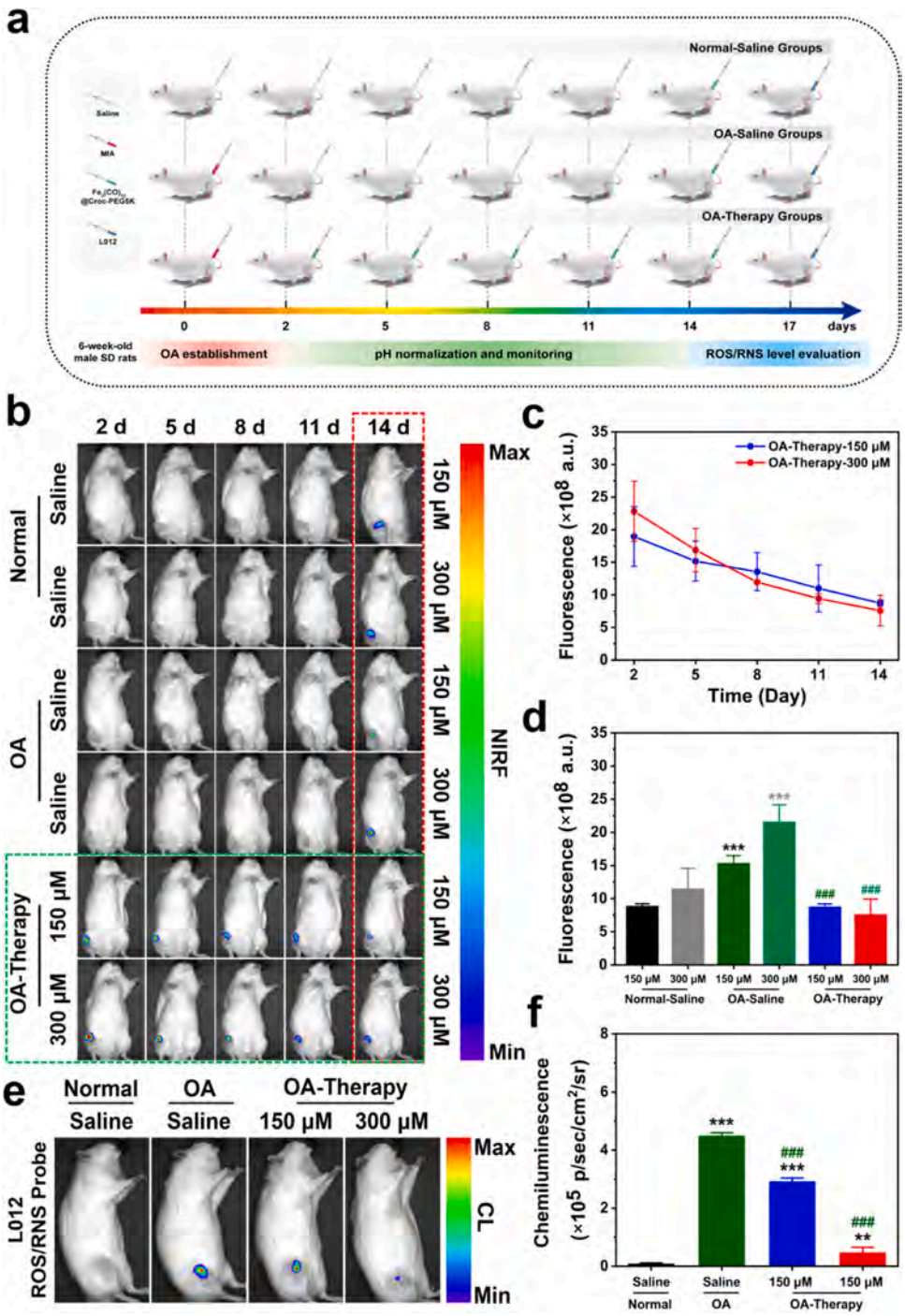

Fig. 8. *In vivo* NIRF imaging and ROS/RNS scavenging characteristics of $Fe_3(CO)_{12}$ @Croc-PEG5K. (a) Schematic diagram of the experimental procedures; (b) NIRF images of rats in different groups after each intra-articular injection; (c) Corresponding NIRF intensities of rats in OA-Therapy groups at different time points; (d) Corresponding NIRF intensity of rats in different groups after final injection of $Fe_3(CO)_{12}$ @Croc-PEG5K; (e) ROS/RNS CL images of rats after different therapies; (f) Corresponding CL intensities of rats after different therapies. $^{*}P < 0.05$, $^{**}P < 0.01$, $^{***}P < 0.001$, relative to the Normal-Saline group, $^{\#}P < 0.05$, $^{\#\#}P < 0.01$, $^{\#\#\#}P < 0.001$, relative to the OA-Saline group.

chondrocytes proliferation (Fig. 3b), but also indirectly protect chondrocytes by regulating macrophages.

In vivo microenvironment monitoring and normalization of $Fe_3(CO)_{12}$ @Croc-PEG5K

Based on the promising *in vitro* results, the therapeutic effect of $Fe_3(CO)_{12}$ @Croc-PEG5K is evaluated *in vivo* using OA rats as the animal model. After intra-articular injection, the retention time of $Fe_3(CO)_{12}$ @Croc-PEG5K in the articular cavity is indicated by fluorescence (Fig. S18), and the administration interval of $Fe_3(CO)_{12}$ @Croc-PEG5K is determined to be 72 h for the *in vivo* study. The NIRF images of the isolated organs reveal high accumulation in the kidney, suggesting that $Fe_3(CO)_{12}$ @Croc-PEG5K is mainly evacuated through the renal system (Fig. S19).

Furthermore, on account of the pH sensitivity (the lower the pH, the stronger the NIRF intensity) and ROS/RNS scavenging of $Fe_3(CO)_{12}$ @Croc-PEG5K, the therapeutic process can be monitored in real-time.

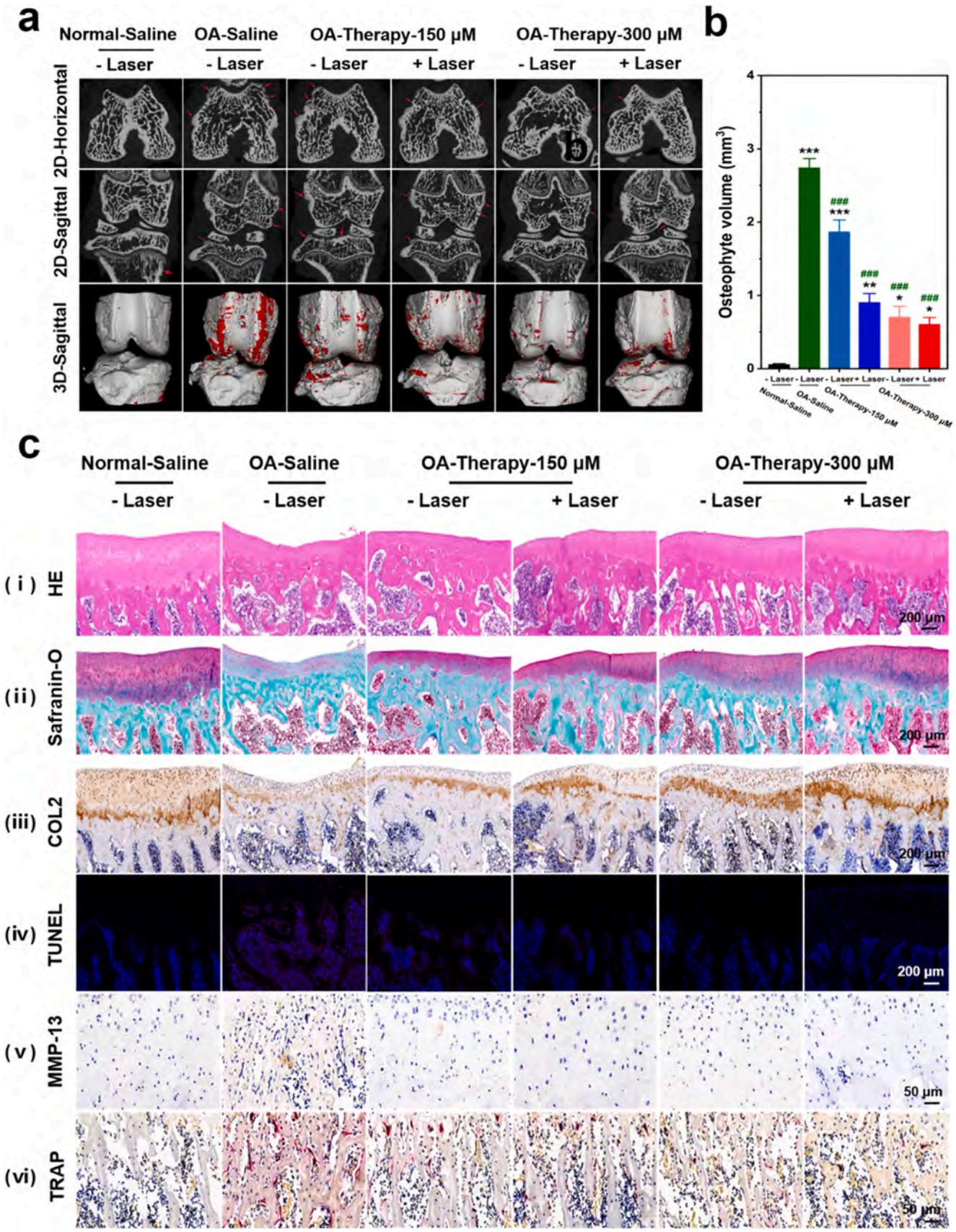

Fig. 9. *In vivo* therapeutic efficacy of $Fe_3(CO)_{12}$ @Croc-PEG5K. (a) Micro-CT images and (b) osteophyte volume after different treatments; (c) Histological staining [(i) HE and (ii) Safranin-O)] and immunohistochemical staining [(iii) Collagen II, (vi) TUNEL, (v) MMP-13 and (vi) TRAP] after different treatments. $^{*}P < 0.05$, $^{**}P < 0.01$, $^{***}P < 0.001$, relative to the Normal-Saline group without laser irradiation, $^{\#}P < 0.05$, $^{\#\#}P < 0.01$, $^{\#\#\#}P < 0.001$, relative to the OA-Saline group without laser irradiation.

The OA rats in the OA-Therapy groups are treated with 150 μM or 300 μM $Fe_3(CO)_{12}$ @Croc-PEG5K every 3 days. For easy comparison, both the normal and OA rats are parallelly treated with sterilized saline and designated as the Normal-Saline group and OA-Saline group, respectively (Fig. 8a). For the OA-Therapy groups (green wireframe), a gradual decrease in the *in vivo* NIRF intensity is observed after each injection, indicating that the inflammatory microenvironment with weak acidity is relieved (Fig. 8b, c). At the last time point, all the rats from different groups are injected with $Fe_3(CO)_{12}$ @Croc-PEG5K for the final evaluation of the therapeutic effect by NIRF imaging (red wireframe). The results show that the *in vivo* NIRF density of the OA rats after periodic $Fe_3(CO)_{12}$ @Croc-PEG5K treatments is significantly lower than that of the OA-Saline group, which is at the same level as the Normal-Saline group (Fig. 8d). Furthermore, $Fe_3(CO)_{12}$ @Croc-PEG5K has the desirable free radical scavenging capacity *in vivo*, as demonstrated by the lower ROS/RNS levels in the OA-Therapy groups compared to the OA-Saline group (Fig. 8e, f). Hence, $Fe_3(CO)_{12}$ @Croc-PEG5K ameliorates the pathological microenvironment under OA conditions by scavenging free ROS/RNS and regulating pH. The therapeutic process can be evaluated by NIRF imaging due to the pH response, so that OA treatment and monitoring can be performed simultaneously.

In vivo therapeutic efficacy of $Fe_3(CO)_{12}$ @Croc-PEG5K

Thermotherapy can improve blood circulation, disperse stasis, reduce swelling, and relieve pain. Here, CO release from $Fe_3(CO)_{12}$ @Croc-PEG5K can also be mediated by photothermal stimulation. Fig. S20 shows that the temperature at the articular cavities with 150 μM and 300 μM $Fe_3(CO)_{12}$ @Croc-PEG5K upon 10-min NIR irradiation (1.0 W/cm^2) reaches 38.9 °C and 42.1 °C, respectively. The moderate photothermal effect together with CO release ameliorates the pathological microenvironment in the OA rats to delay the degradation of cartilage and reduce the formation of osteophytes (Fig. 9a, b). After different therapies, the cartilage protective effect is investigated by histological and immunohistochemical staining. As shown in Fig. 9c i, the hematoxylin-eosin (HE) stained image of the OA-Saline group exhibits surface irregularity, matrix degradation, and structural damage typical of OA. Glycosaminoglycan is abundant in the cartilage and matrix. The amount of glycosaminoglycan (stained in red) is the smallest in the OA-Saline group, while administration of $Fe_3(CO)_{12}$ @Croc-PEG5K alleviates the degeneration of glycosaminoglycan in a dose and NIR-dependent manner (Fig. 9c ii). The expression of collagen II (a major biomarker of cartilage, stained in brown in Fig. 9c iii) in the OA-Saline group is much lower than that in the Normal-Saline group. In contrast, in the OA-Therapy groups, especially the group with high-dose of $Fe_3(CO)_{12}$ @Croc-PEG5K and laser irradiation, more collagen II expression is observed.

To observe apoptosis of chondrocytes, TUNEL staining is performed, and positive result (stained in red) is only observed from the OA-Saline group (Fig. 9c iv). MMP-13 is a kind of matrix metalloproteinase that has a strong destructive effect on the cartilage matrix. As shown in Fig. 9c v, the secretion levels of MMP-13 (stained in brown) in the OA-Therapy groups are lower than that of the OA-Saline group, indicating better preservation of the cartilage. Osteoclasts can break down and digest hydrated proteins and minerals by secreting acids and collagenase, leading to the degradation of subchondral bone and cartilage. The results of tartrate-resistant acid phosphatase (TRAP) staining demonstrate that the $Fe_3(CO)_{12}$ @Croc-PEG5K treatment decreases the activity of osteoclasts (stained in red), which is desirable for joint protection (Fig. 9c vi). These results corroborate that the administration of $Fe_3(CO)_{12}$ @Croc-PEG5K protects the articular cartilage from continuous deterioration under OA conditions, and proper NIR irradiation further enhances the therapeutic efficacy. After different therapies, the levels of alanine transaminase (ALT), aspartate transaminase (AST), blood urea nitrogen (BUN), creatinine (CREA), platelets (PLT), and white blood cells (WBC) are evaluated, and no significant difference can be found between the OA-Therapy groups and Normal-Saline group (Fig. S21). Additionally, the $Fe_3(CO)_{12}$ @Croc-PEG5K treatment causes negligible damage or inflammation in the main organs of the experimental rats consequently confirming the *in vivo* biosafety of $Fe_3(CO)_{12}$ @Croc-PEG5K (Fig. S22).

Conclusion

An intelligent cascade-responsive nano gas tank, $Fe_3(CO)_{12}$ @Croc-PEG5K, is designed and demonstrated for the auto-diagnosis and precision treatment of OA. As a therapeutic agent, $Fe_3(CO)_{12}$ @Croc-PEG5K releases CO for gas therapy under photothermal stimulation, scavenges free radicals (ROS/RNS) in the articular microenvironment, and inhibits excessive inflammation of OA to preserve the structural integrity of the articular cartilage. As a diagnostic agent, it can be used to optimize the administration window and monitor the therapeutic process by NIRF imaging. Our study for the first time validates the effects of CO gas therapy in OA, especially in an imaging-guided way, thus providing new information and insights into the refinement of OA treatment.

CRediT authorship contribution statement

Huaiyu Wang, Xiaoting Gao: Conceptualization. **Huaiyu Wang, Xiaoting Gao, Wei Zhang, Ruiqiang Hang, Liping Tong**: Methodology. **Xiaoting Gao, Lei Yan, Yuanliang Lv, Peiyan Ou, Ang Gao**: Investigation. **Huaiyu Wang**: Supervision. **Xiaoting Gao**: Writing—original draft. **Paul K. Chu, Huaiyu Wang**: Writing—review & editing.

Declaration of Competing Interest

The authors declare that they have no known competing financial interests or personal relationships that could have appeared to influence the work reported in this paper.

Data availability

Data will be made available on request.

Acknowledgments

This work was financially supported by the National Key Research and Development Program of China (2021YFB3800800), National Natural Science Foundation of China (82272157), Shenzhen Science and Technology Research Funding (JSGG20200225152648408), Guang Dong Basic and Applied Basic Research Foundation (2022B1515130010).

Appendix A. Supporting information

Supplementary data associated with this article can be found in the online version at doi:10.1016/j.nantod.2023.102047.

References

[1] H. Weinans, M. Siebelt, R. Agricola, S.M. Botter, T.M. Piscaer, J.H. Waarsing, Pathophysiology of peri-articular bone changes in osteoarthritis, Bone 51 (2012) 90–196.
[2] F.J. Blanco, R. Guitian, E. Vazquez-Martul, F.J. de Toro, F. Galdo, Osteoarthritis chondrocytes die by apoptosis. A possible pathway for osteoarthritis pathology, Arthritis Rheumatol. 41 (1998) 284–289.
[3] K. McCulloch, G.J. Litherland, T.S. Rai, Cellular senescence in osteoarthritis pathology, Aging Cell 16 (2017) 210–218.
[4] M. Kapoor, J. Martel-Pelletier, D. Lajeunesse, J.P. Pelletier, H. Fahmi, Role of proinflammatory cytokines in the pathophysiology of osteoarthritis, Nat. Rev. Rheumatol. 7 (2011) 33–42.
[5] K.D. Allen, L.M. Thoma, Y.M. Golightly, Epidemiology of osteoarthritis, Osteoarthr. Cartil. 30 (2022) 184–195.

[6] A.Y.N. Lim, M. Doherty, What of guidelines for osteoarthritis? Int. J. Rheum. Dis. 14 (2011) 136–144.
[7] Q. Liu, S. Wang, J. Lin, Y. Zhang, The burden for knee osteoarthritis among Chinese elderly: estimates from a nationally representative study, Osteoarthr. Cartil. 26 (2018) 1636–1642.
[8] C. Mora, R. Przkora, Y. Cruz-Almeida, Knee osteoarthritis: pathophysiology and current treatment modalities, J. Pain Res. 11 (2018) 2189–2196.
[9] M. Englund, F.W. Roemer, D. Hayashi, M.D. Crema, A. Guermazi, Meniscus pathology, osteoarthritis and the treatment controversy, Nat. Rev. Rheumatol. 8 (2012) 412–419.
[10] L.F. Kou, S.Y. Xiao, R. Sun, S.H. Bao, Q. Yao, R.J. Chen, Biomaterial-engineered intra-articular drug delivery systems for osteoarthritis therapy, Drug Deliv. 26 (2019) 870–885.
[11] G. Jamtvedt, K.T. Dahm, A. Christie, R.H. Moe, E. Haavardsholm, I. Holm, K. B. Hagen, Physical therapy interventions for patients with osteoarthritis of the knee: an overview of systematic reviews, Phys. Ther. 88 (2008) 123–136.
[12] G.D. Deyle, N.E. Henderson, R.L. Matekel, M.G. Ryder, M.B. Garber, S.C. Allison, Effectiveness of manual physical therapy and exercise in osteoarthritis of the knee. A randomized, controlled trial, Ann. Intern. Med. 132 (2000) 173–181.
[13] L.O. Dantas, T.D. Salvini, T.E. McAlindon, Knee osteoarthritis: key treatments and implications for physical therapy, Braz. J. Phys. Ther. 25 (2021) 135–146.
[14] G.K. Fitzgerald, C. Oatis, Role of physical therapy in management of knee osteoarthritis, Curr. Opin. Rheumatol. 16 (2004) 143–147.
[15] K.L. Bennell, T. Egerton, J. Martin, J.H. Abbott, B. Metcalf, F. McManus, K. Sims, Y. H. Pua, T.V. Wrigley, A. Forbes, C. Smith, A. Harris, R. Buchbinder, Effect of physical therapy on pain and function in patients with hip osteoarthritis: a randomized clinical trial, JAMA 311 (2014) 1987–1997.
[16] H.N. Peng, A.C. Ou, X.H. Huang, C. Wang, L. Wang, T.B. Yu, Y.Z. Zhang, Y. Zhang, Osteotomy around the knee: the surgical treatment of osteoarthritis, Orthop. Surg. 13 (2021) 1465–1473.
[17] P. Dieppe, K. Lim, S. Lohmander, Who should have knee joint replacement surgery for osteoarthritis? Int. J. Rheum. Dis. 14 (2011) 175–180.
[18] A. W-Dahl, O. Robertsson, L. Lidgren, Surgery for knee osteoarthritis in younger patients, Acta Orthop. 81 (2010) 161–164.
[19] J. Lutzner, P. Kasten, K.P. Gunther, S. Kirschner, Surgical options for patients with osteoarthritis of the knee, Nat. Rev. Rheumatol. 5 (2009) 309–316.
[20] G.L. Matthews, D.J. Hunter, Emerging drugs for osteoarthritis, Expert Opin. Emerg. Drugs 16 (2011) 479–491.
[21] I.A. Jones, R. Togashi, M.L. Wilson, N. Heckmann, C.T. Vangsness, Intra-articular treatment options for knee osteoarthritis, Nat. Rev. Rheumatol. 15 (2019) 77–90.
[22] A. Latourte, M. Kloppenburg, P. Richette, Emerging pharmaceutical therapies for osteoarthritis, Nat. Rev. Rheumatol. 16 (2020) 673–688.
[23] D.J. Hunter, Pharmacologic therapy for osteoarthritis–the era of disease modification, Nat. Rev. Rheumatol. 7 (2011) 13–22.
[24] S. Kennedy, J.R.S. Tambiah, N.E. Lane, Osteoarthritis today: lost in translation, Best. Pract. Res. Cl. Rh. 36 (2022), 101810.
[25] Y.J. Liang, X. Xu, L.M. Xu, I. Prasadam, L. Duan, Y. Xiao, J. Xia, Non-surgical osteoarthritis therapy, intra-articular drug delivery towards clinical applications, J. Drug Target. 29 (2021) 609–616.
[26] C.K. O'Neil, J.T. Hanlon, Z.A. Marcum, Adverse effects of analgesics commonly used by older adults with osteoarthritis: focus on non-opioid and opioid analgesics, Am. J. Geriatr. Pharmacother. 10 (2012) 331–342.
[27] C.H. Ding, Do NSAIDs affect the progression of osteoarthritis? Inflammation 26 (2002) 139–142.
[28] Y. Xu, Y. Li, A. Gao, P.K. Chu, H. Wang, Gasotransmitter delivery for bone diseases and regeneration, Innov. Life 1 (2023), 100015.
[29] S. Tao, J. Cheng, G. Su, D. Li, Z. Shen, F. Tao, T. You, J. Hu, Breathing Micelles for combinatorial treatment of rheumatoid arthritis, Angew. Chem. Int. Ed. 59 (2020) 21864–21869.
[30] W.L. Wan, Y.J. Lin, P.C. Shih, Y.R. Bow, Q. Cui, Y. Chang, W.T. Chia, H.W. Sung, An insitu depot for continuous evolution of gaseous H2 mediated by a magnesium passivation/activation cycle for treating osteoarthritis, Angew. Chem. Int. Ed. 130 (2018) 10023–10027.
[31] K. Ling, F. Men, W.C. Wang, Y.Q. Zhou, H.W. Zhang, D.W. Ye, Carbon monoxide and its controlled release: therapeutic application, detection, and development of carbon monoxide releasing molecules (CORMs), J. Med. Chem. 61 (2018) 2611–2635.
[32] W. Durante, Carbon monoxide and bile pigments: surprising mediators of vascular function, Vasc. Med. 7 (2002) 195–202.
[33] M.L. Ferrandiz, N. Maicas, I. Garcia-Amandis, M.C. Terencio, R. Motterlini, I. Devesa, L.A.B. Joosten, W.B. van den Berg, M.J. Alcaraz, Treatment with a CO-releasing molecule (CORM-3) reduces joint inflammation and erosion in murine collagen-induced arthritis, Ann. Rheum. Dis. 67 (2008) 1211–1217.
[34] S. Mishra, T. Fujita, V.N. Lama, D. Nam, H. Liao, M. Okada, K. Minamoto, Y. Yoshikawa, H. Harada, D.J. Pinsky, Carbon monoxide rescues ischemic lungs by interrupting MAPK-driven expression of early growth response 1 gene and its downstream target genes, Proc. Natl. Acad. Sci. USA 103 (2006) 5191–5196.
[35] B. Wegiel, D.J. Gallo, K.G. Raman, J.M. Karlsson, B. Ozanich, B.Y. Chin, E. Tzeng, S. Ahmad, A. Ahmed, C.J. Baty, L.E. Otterbein, Nitric oxide-dependent bone marrow progenitor mobilization by carbon monoxide enhances endothelial repair after vascular injury, Circulation 121 (2010) 537–548.
[36] S. Coaccioli, P. Sarzi-Puttini, P. Zis, G. Rinonapoli, G. Varrassi, Osteoarthritis: new insight on its pathophysiology, J. Clin. Med. 11 (2022) 6013.
[37] B. Abramoff, F.E. Caldera, Osteoarthritis: pathology, diagnosis, and treatment options, Med. Clin. North Am. 104 (2020) 293–311.
[38] S.M. Hussain, C. Dawson, Y.Y. Wang, A.M. Tonkin, L. Chou, A.E. Wluka, F. M. Cicuttini, Vascular pathology and osteoarthritis: a systematic review, J. Rheumatol. 47 (2020) 748–760.
[39] J.A. Guzman, Carbon monoxide poisoning, Crit. Care Clin. 28 (2012) 537–548.
[40] C. Mattiuzzi, G. Lippi, Worldwide epidemiology of carbon monoxide poisoning, Hum. Exp. Toxicol. 39 (2020) 387–392.
[41] G. Reumuth, Z. Alharbi, K.S. Houschyar, B.S. Kim, F. Siemers, P.C. Fuchs, G. Grieb, Carbon monoxide intoxication: what we know, Burns 45 (2019) 526–530.
[42] Y. Zhou, W. Yu, J. Cao, H. Gao, Harnessing carbon monoxide-releasing platforms for cancer therapy, Biomaterials 255 (2020), 120193.
[43] L.S. Lazarus, A.D. Benninghoff, L.M. Berreau, Development of triggerable, trackable, and targetable carbon monoxide releasing molecules, Acc. Chem. Res. 53 (2020) 2273–2285.
[44] S. Garcia-Gallego, G.J.L. Bernardes, Carbon-monoxide-releasing molecules for the delivery of therapeutic CO in vivo, Angew. Chem. Int. Ed. 53 (2014) 9712–9721.
[45] I. Chakraborty, S.J. Carrington, P.K. Mascharak, Design strategies to improve the sensitivity of photoactive metal carbonyl complexes (photoCORMs) to visible light and their potential as CO-donors to biological targets, Acc. Chem. Res. 47 (2014) 2603–2611.
[46] Z. Jin, Y. Wen, L. Xiong, T. Yang, P. Zhao, L. Tan, T. Wang, Z. Qian, B.L. Su, Q. He, Intratumoral H(2)O(2)-triggered release of CO from a metal carbonyl-based nanomedicine for efficient CO therapy, Chem. Commun. 53 (2017) 5557–5560.
[47] S. Romanski, B. Kraus, U. Schatzschneider, J.M. Neudorfl, S. Amslinger, H. G. Schmalz, Acyloxybutadiene iron tricarbonyl complexes as enzyme-triggered CO-releasing molecules (ET-CORMs), Angew. Chem. Int. Ed. 50 (2011) 2392–2396.
[48] Q. He, D.O. Kiesewetter, Y. Qu, X. Fu, J. Fan, P. Huang, Y. Liu, G. Zhu, Y. Liu, Z. Qian, X. Chen, NIR-responsive on-demand release of CO from metal carbonyl-caged graphene oxide nanomedicine, Adv. Mater. 27 (2015) 6741–6746.
[49] J. Meng, Z. Jin, P. Zhao, B. Zhao, M. Fan, Q. He, Sci. Adv. 6 (2020), eaba1362.
[50] G. Ma, Z. Liu, C. Zhu, H. Chen, R.T.K. Kwok, P. Zhang, B.Z. Tang, L. Cai, P. Gong, Angew. Chem. Int. Ed. 61 (2022), e202207213.
[51] X. Gao, S. Jiang, C. Li, Y. Chen, Y. Zhang, P. Huang, J. Lin, Highly photostable croconium dye-anchored cell membrane vesicle for tumor pH-responsive duplex imaging-guided photothermal therapy, Biomaterials 267 (2021), 120454.
[52] W. Jiang, Z. Shen, Z. Guo, Q. Wang, Q. Li, J. Hu, Y. Wang, Overcoming oxygen heterogeneity of tumor microenvironments to boost cancer immunotherapy by oxygen-switchable ROS/RNS nanogenerators, Nano Today 48 (2023), 101696.
[53] X. Wang, H. Zhao, Z. Liu, Y. Wang, S.G. Shen, Field application of star polymer-delivered chitosan to amplify plant defense against potato late blight, Chem. Eng. J. 417 (2021), 129284.
[54] J. Ruan, Q. Yu, H. Cui, X. Qin, L. Qin, S. Chen, D. Niu, C. Fan, Appl. Mater. Today 25 (2021), 102126.
[55] K. Dhara, S. Lohar, A. Patra, P. Roy, S.K. Saha, G.C. Sadhukhan, P. Chattopadhyay, A new lysosome-targetable turn-on fluorogenic probe for carbon monoxide imaging in living cells, Anal. Chem. 90 (2018) 2933–2938.

Supporting Information

Dual-switched Carbon Monoxide Nano Gas Tank for Auto-Diagnosis and Precision Therapy of Osteoarthritis

Xiaoting Gao [a, b], Lei Yan [a], Wei Zhang [c], Yuanliang Lv [a], Peiyan Ou [a], Ruiqiang Hang [d], Ang Gao [a], Liping Tong [a], Paul K. Chu [e], Huaiyu Wang [a, b, *]

[a] *Center for Human Tissues and Organs Degeneration, Shenzhen Institute of Advanced Technology, Chinese Academy of Sciences, Shenzhen 518055, China*

[b] *University of Chinese Academy of Sciences, Beijing, China*

[c] *Technical Institute of Physics and Chemistry, Chinese Academy of Sciences, Beijing 100080, China*

[d] *Shanxi Key Laboratory of Biomedical Metal Materials, College of Materials Science and Engineering, Taiyuan University of Technology, Taiyuan, 030024, China*

[e] *Department of Physics, Department of Materials Science and Engineering, And Department of Biomedical Engineering, City University of Hong Kong, Tat Chee Avenue, Kowloon, Hong Kong, China*

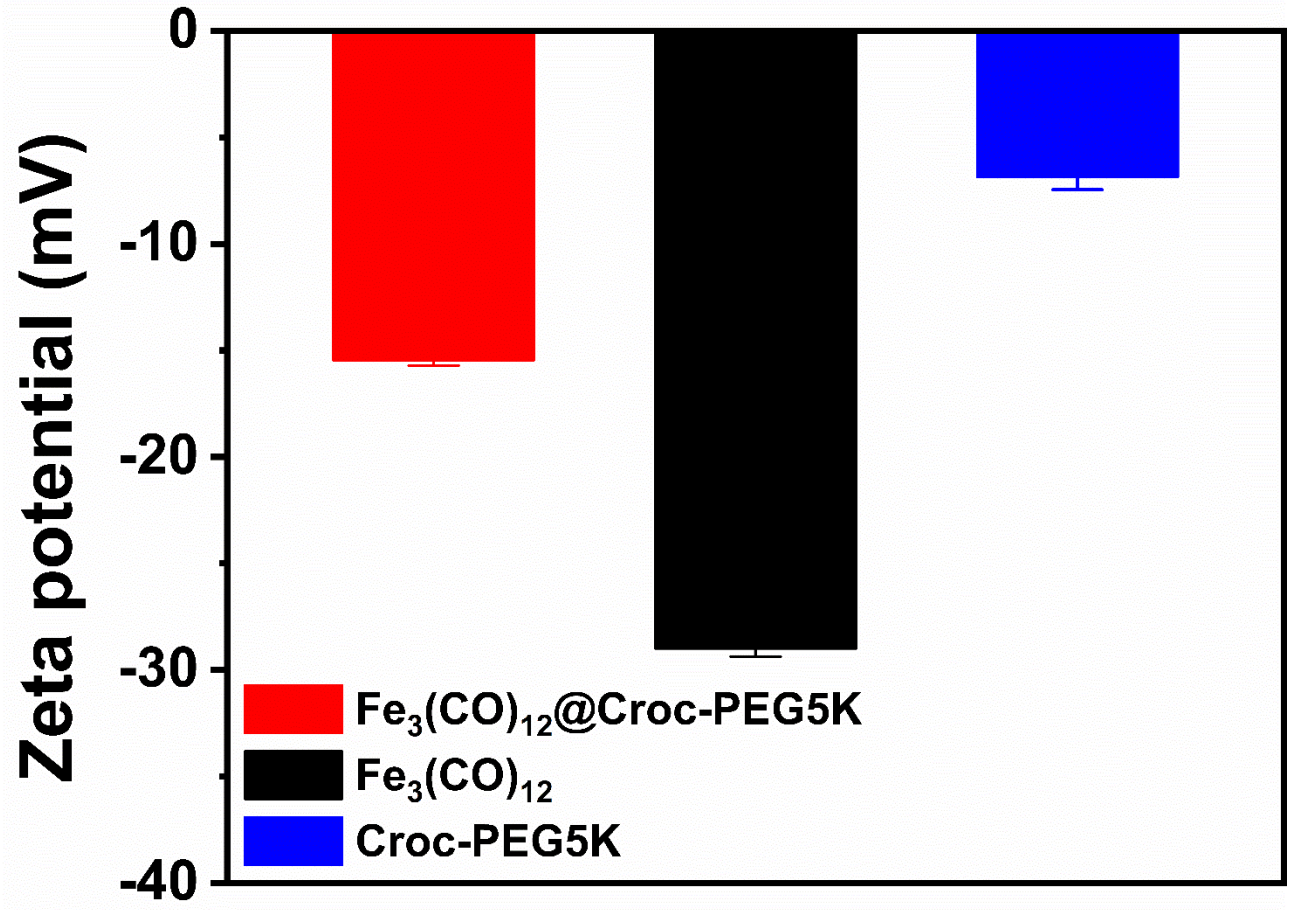

Fig. S1. Zeta potentials of $Fe_3(CO)_{12}$@Croc-PEG5K, $Fe_3(CO)_{12}$ and Croc-PEG5K.

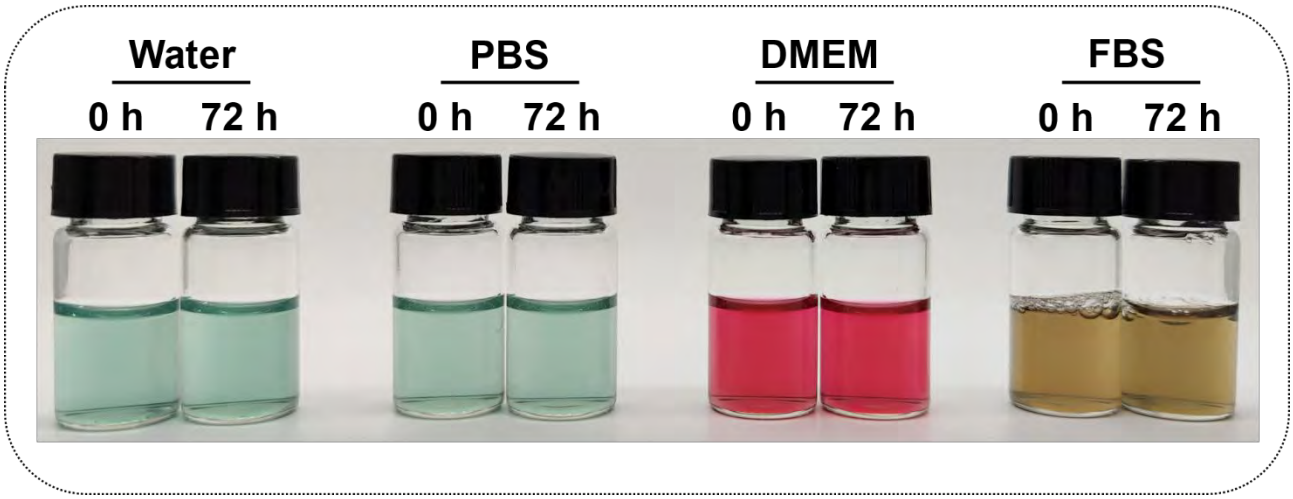

Fig. S2. The dispersion of $Fe_3(CO)_{12}$@Croc-PEG5K in different media (as-prepared and after 72 h).

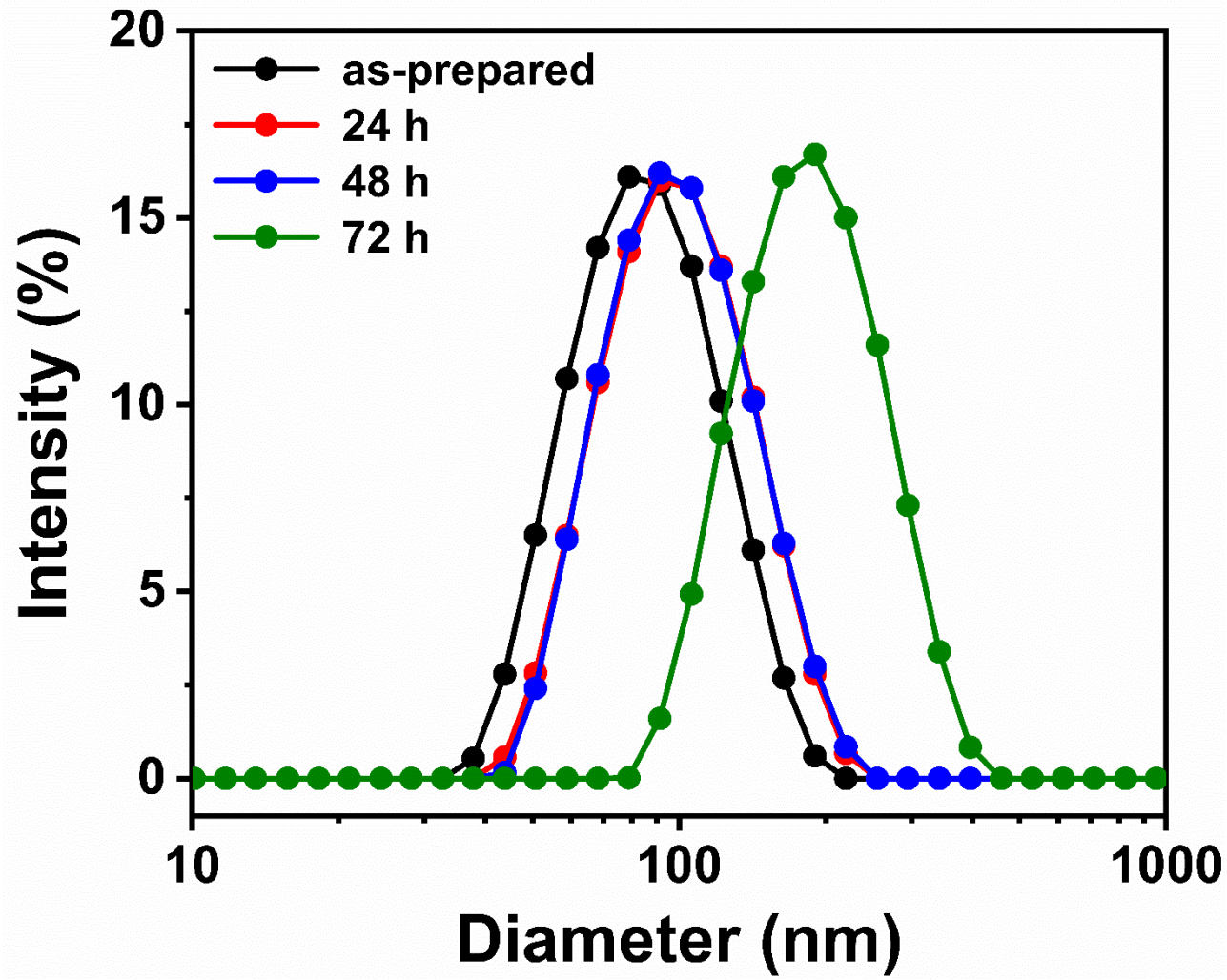

Fig. S3. Dynamic light scattering (DLS) size distribution of $Fe_3(CO)_{12}$@Croc-PEG5K at different time points (as-prepared and after 24, 48 and 72 h).

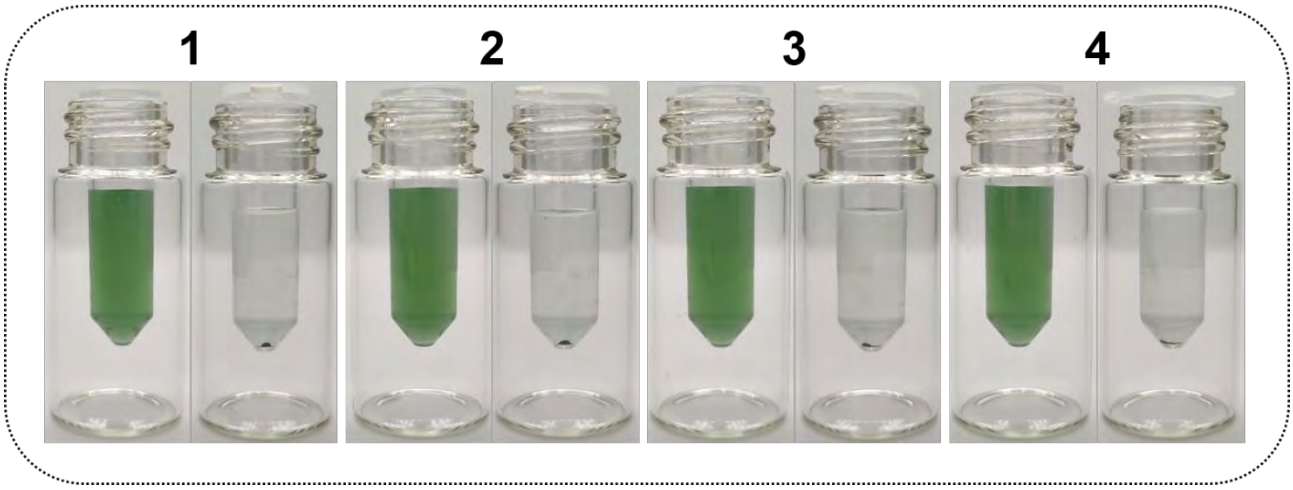

Fig. S4. The stability of $Fe_3(CO)_{12}$@Croc-PEG5K within 4 centrifugation-ultrasonic-resuspension cycles.

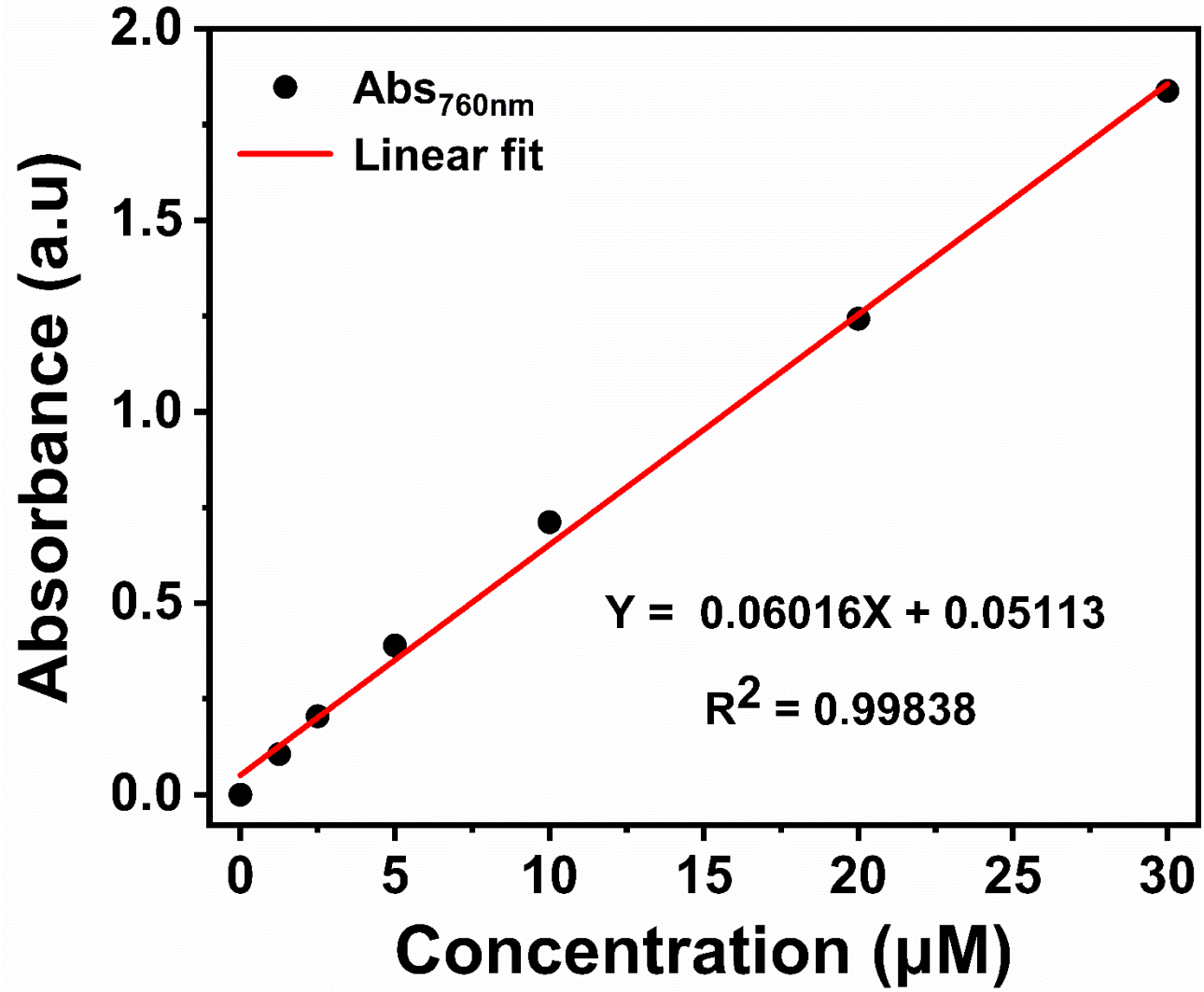

Fig. S5. Croc-PEG5K concentration versus absorbance at 760 nm (Abs_{760}).

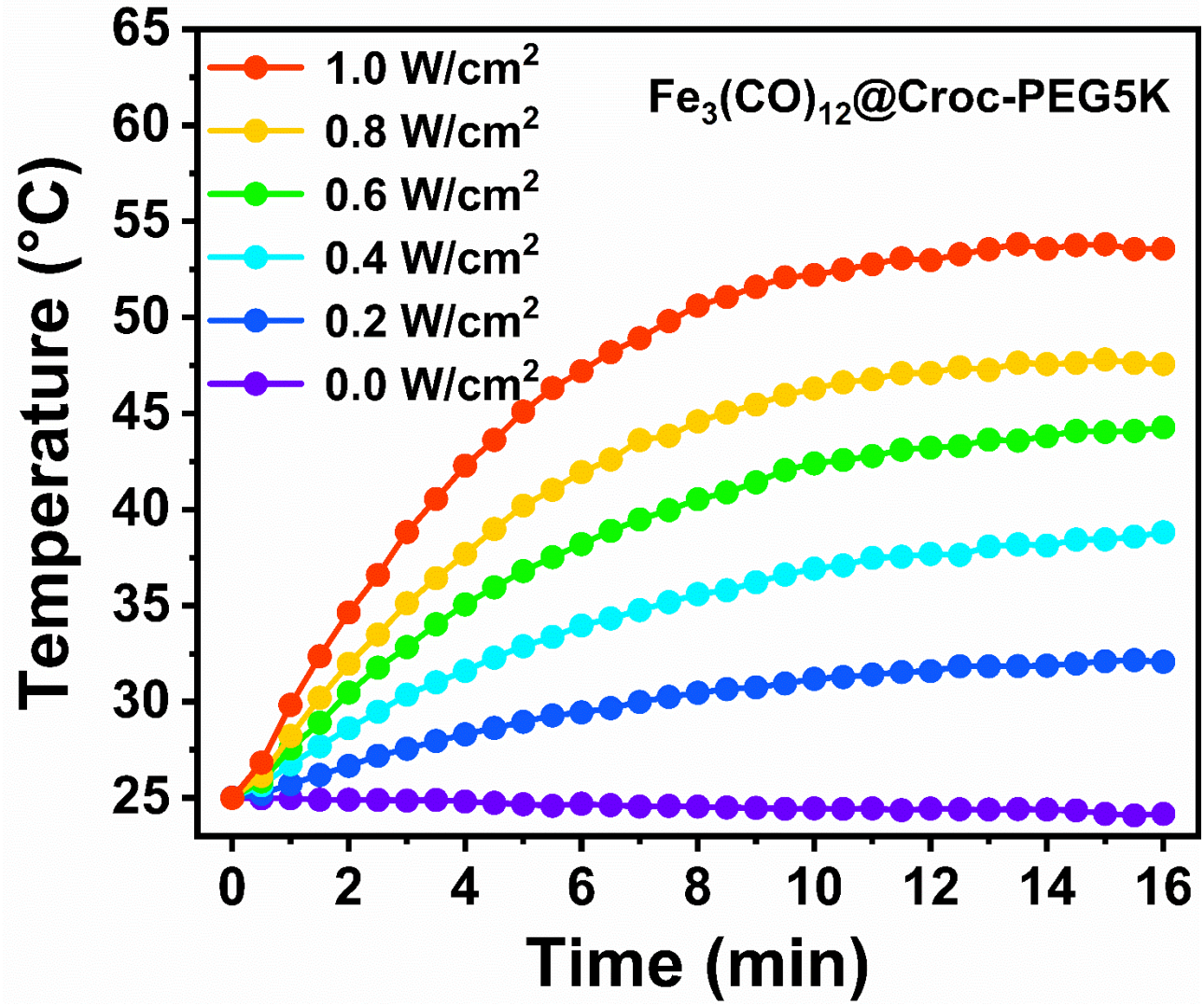

Fig. S6. Temperature evaluation of $Fe_3(CO)_{12}$@Croc-PEG5K (30 μM) under different optical densities (0 ~ 1.0 W/cm^2) of near infrared (NIR) laser irradiation.

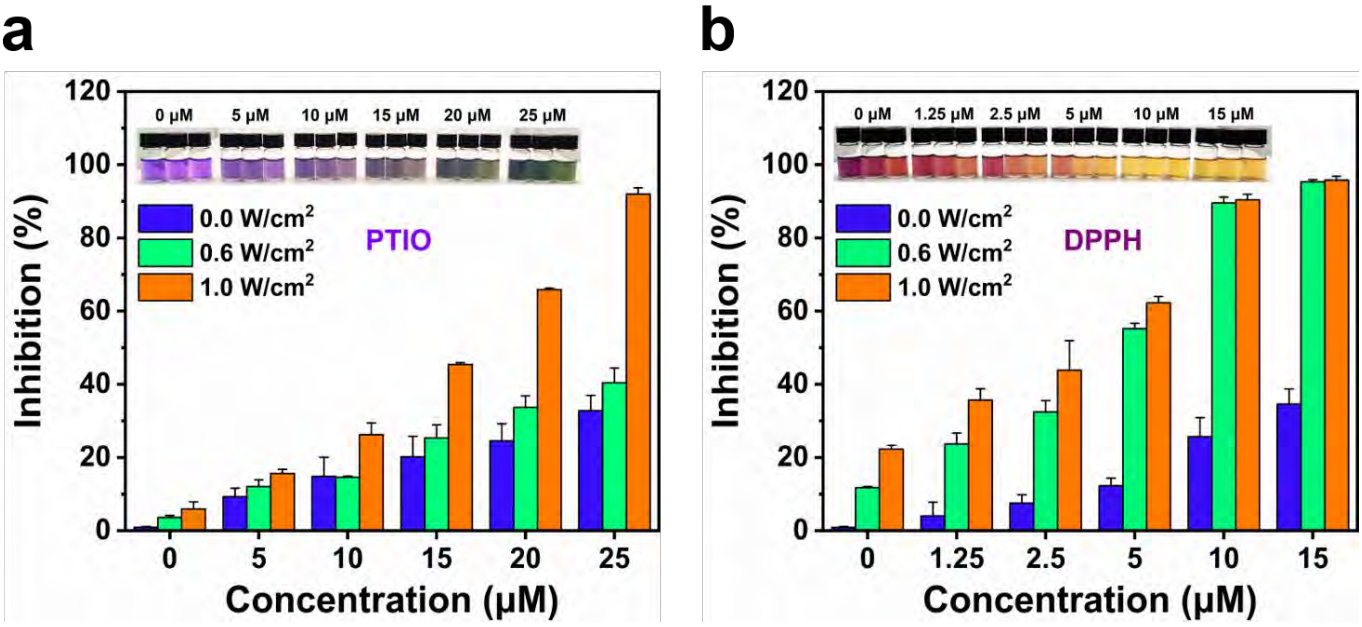

Fig. S7. *In vitro* free radicals: (a) reactive oxide species (ROS) and (b) reactive nitrogen species (RNS) scavenging capacities of $Fe_3(CO)_{12}$@Croc-PEG5K under different optical densities (0 ~ 1.0 W/cm^2) of NIR laser irradiation.

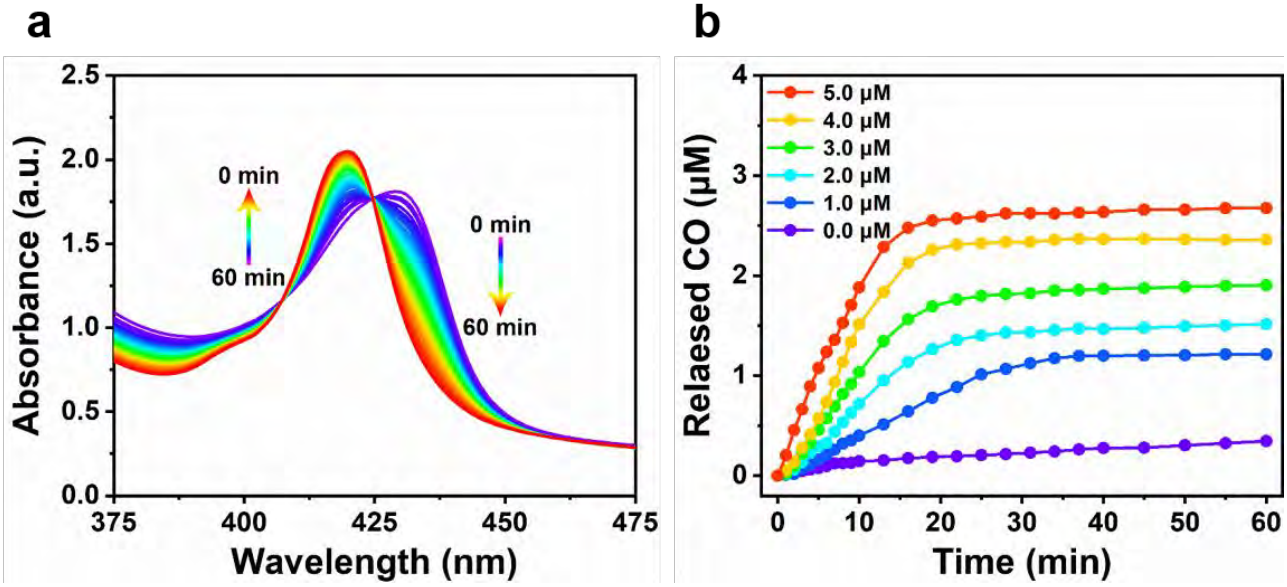

Fig. S8. *In vitro* H_2O_2-mediated CO release of $Fe_3(CO)_{12}$@Croc-PEG5K [Free radical generator: H_2O_2; NIR laser parameter: 808 nm; Solution: $Fe_3(CO)_{12}$@Croc-PEG5K (30 μM) and reduced hemoglobin (Hb, 5 μM) in PBS buffer (pH = 6.8)]. (a) UV-vis-NIR absorption spectra with H_2O_2 (5.0 μM) at different time points (0 ~ 60 min). (b) Time-dependent CO release for different concentrations (0.0 ~ 5.0 W/cm^2) of H_2O_2.

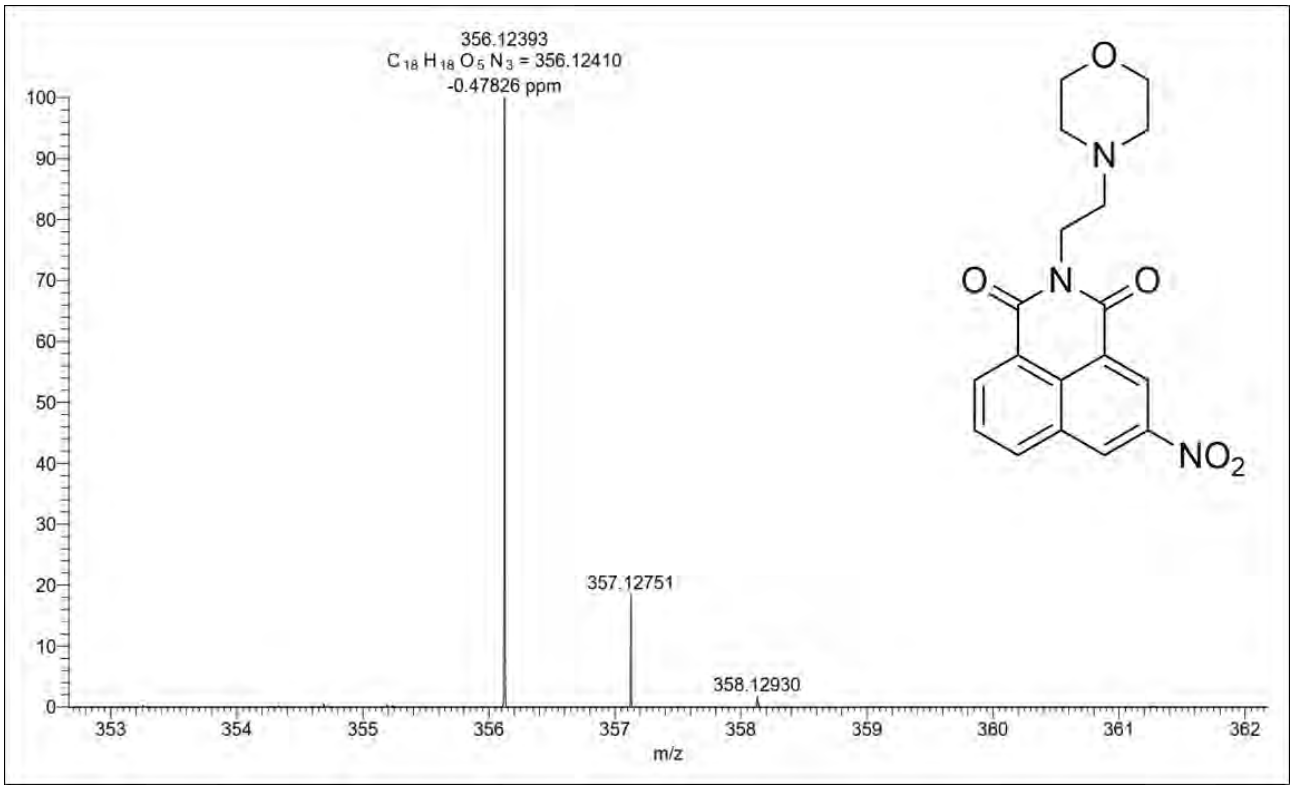

Fig. S9. The high-resolution liquid chromatography-mass (HRLC-MS) spectrum of COP in methanol.

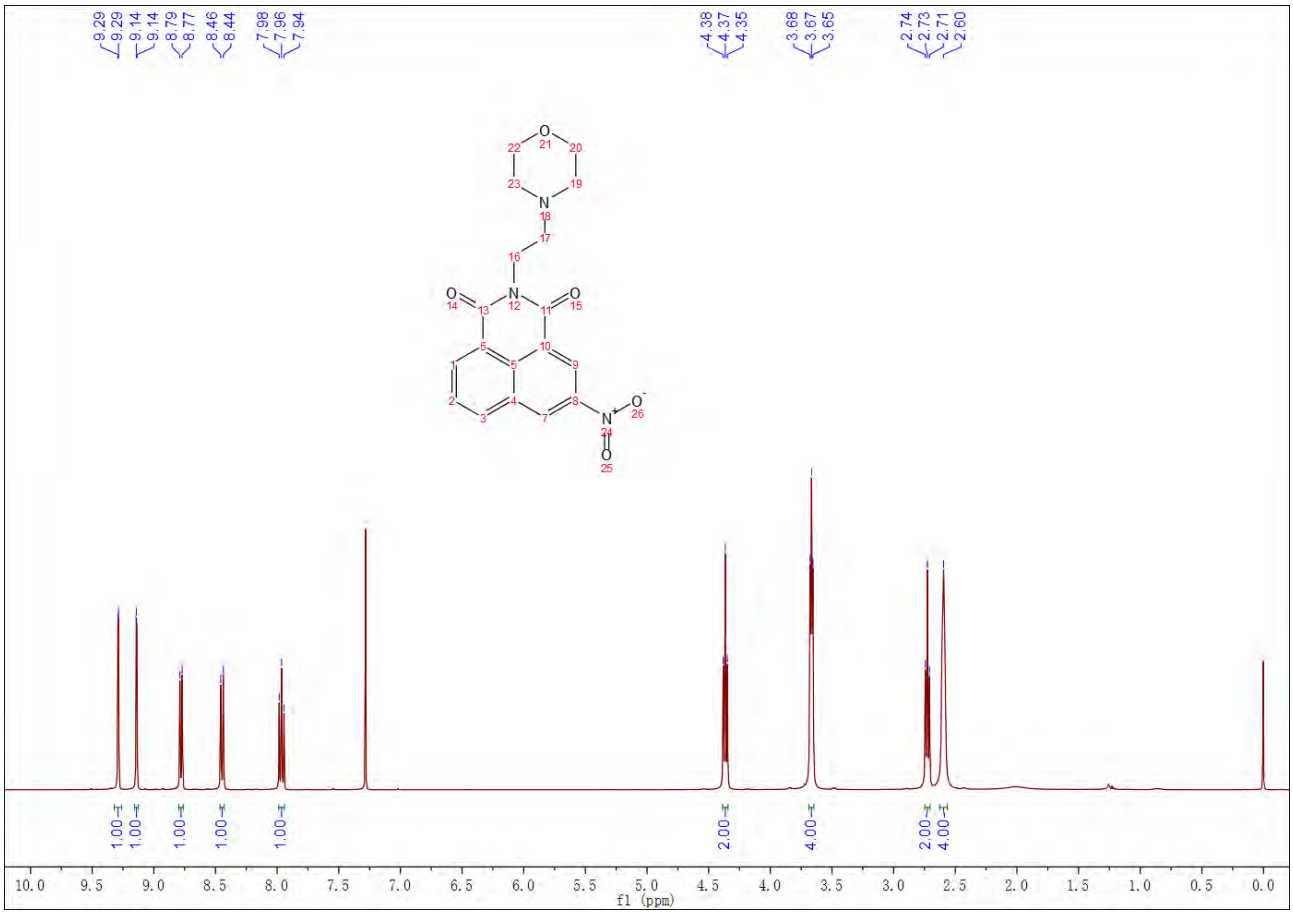

Fig. S10. ^{1}H nuclear magnetic resonance (NMR) spectrum of COP in $CDCl_3$.

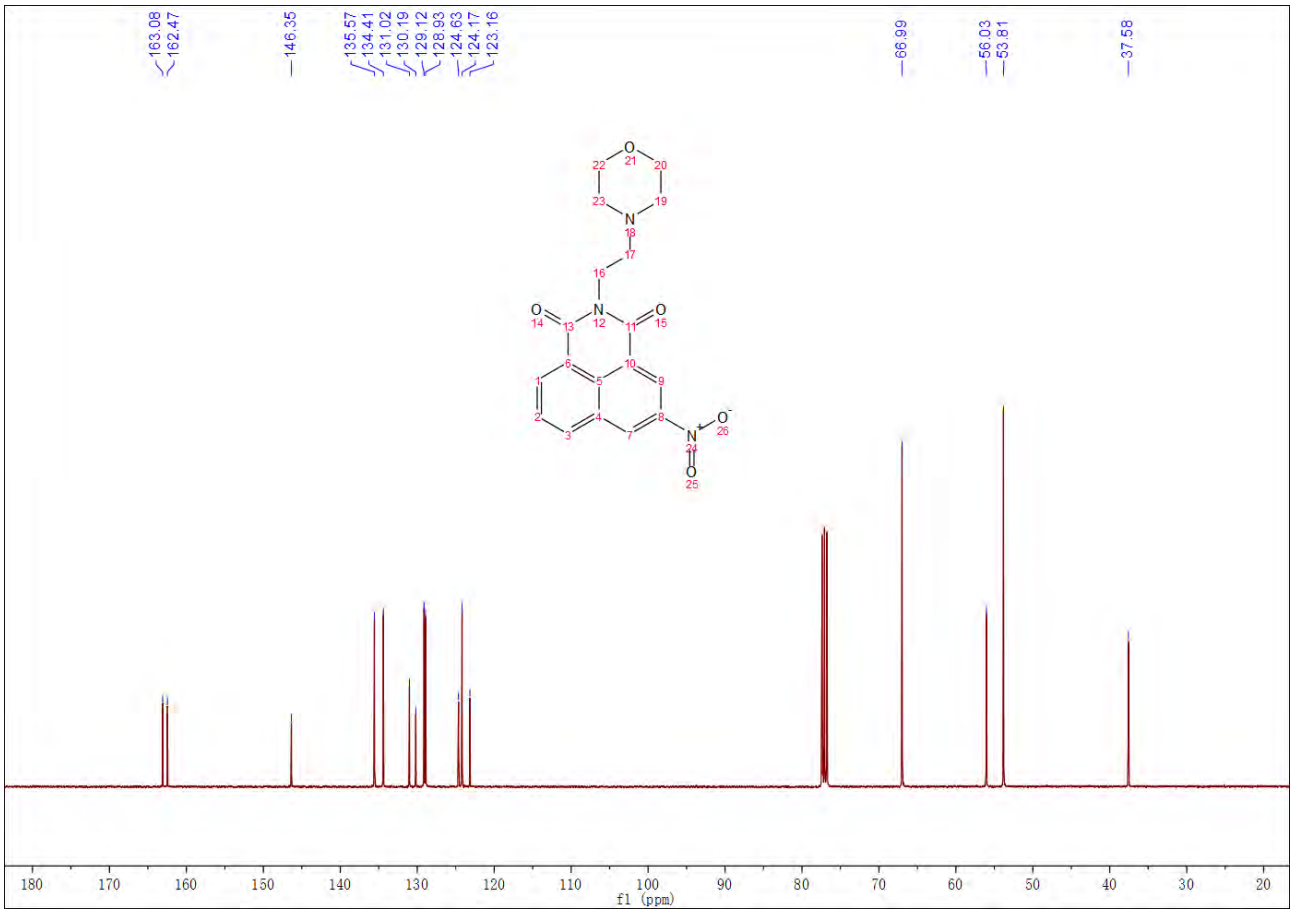

Fig. S11. ^{13}C NMR spectrum of COP in $CDCl_3$.

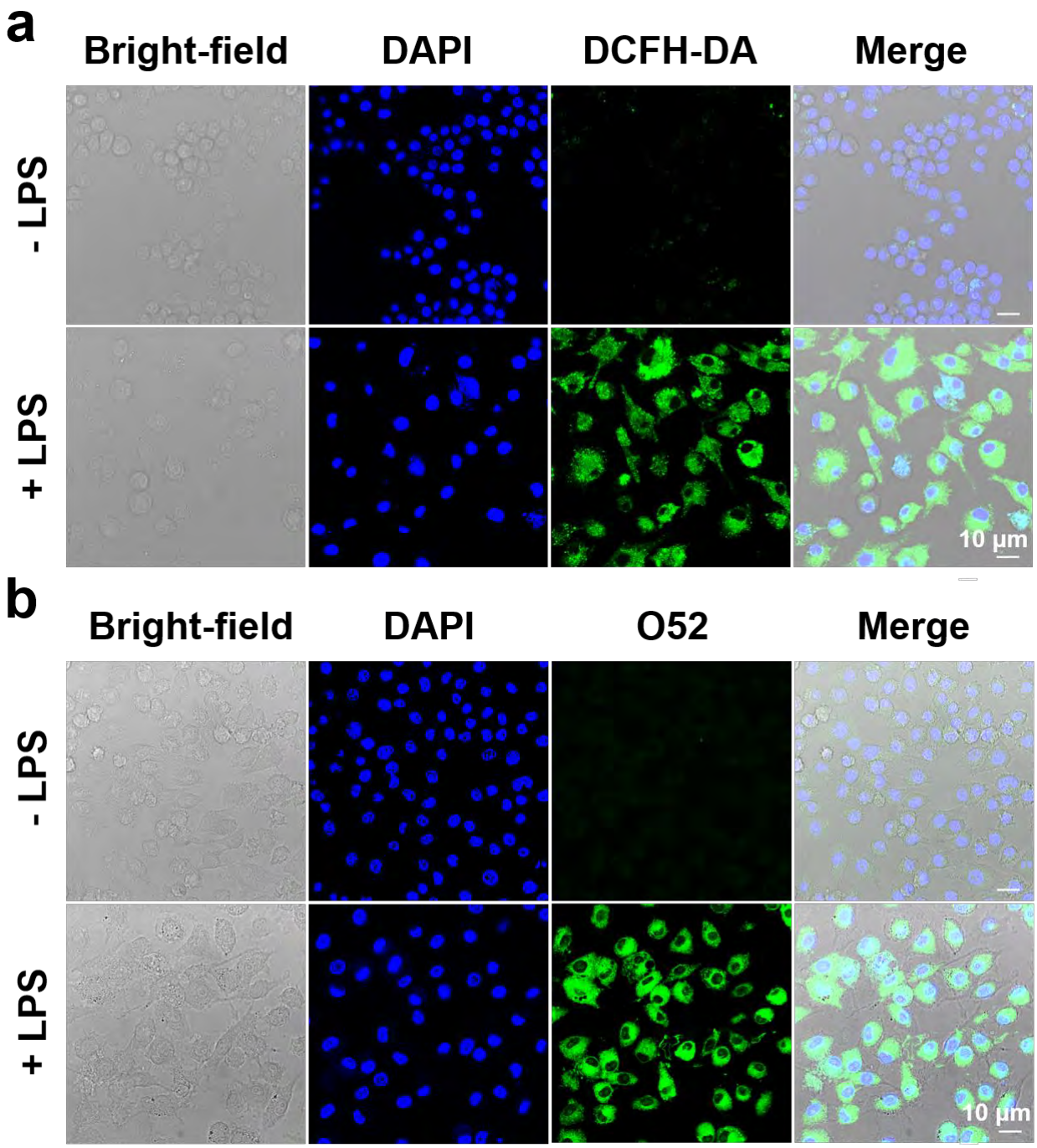

Fig. S12. (a) ROS and (b) RNS levels in Raw264.7 cells with or without LPS stimulation measured by DCFH-DA (ROS probe) and O52 (RNS probe). Blue channel: λex: 405 nm, λem: 437 nm; Green channel: λex: 488 nm, λem: 525 nm (DCFH-DA); λex: 490 nm, λem: 515 nm (O52).

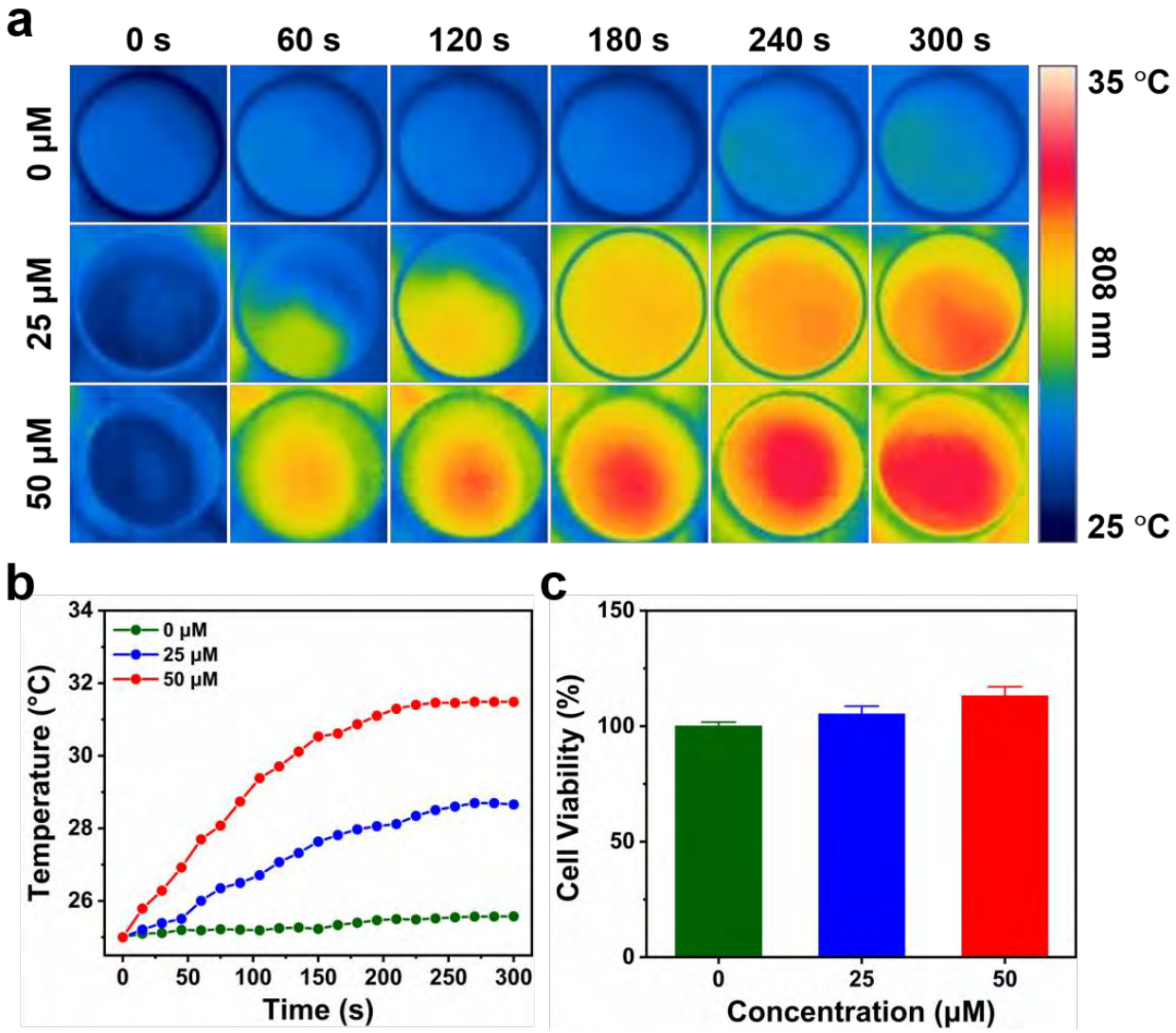

Fig. S13. (a) Thermal images and (b) Temperature changes of Raw264.7 cells with $Fe_3(CO)_{12}$@Croc-PEG5K (25 μM and 50 μM) under NIR laser irradiation (1.0 W/cm^2, 5 min); (c) Effect of $Fe_3(CO)_{12}$@Croc-PEG5K (25 μM and 50 μM) and NIR laser irradiation (1.0 W/cm^2, 5 min) on the viability of Raw264.7 cells.

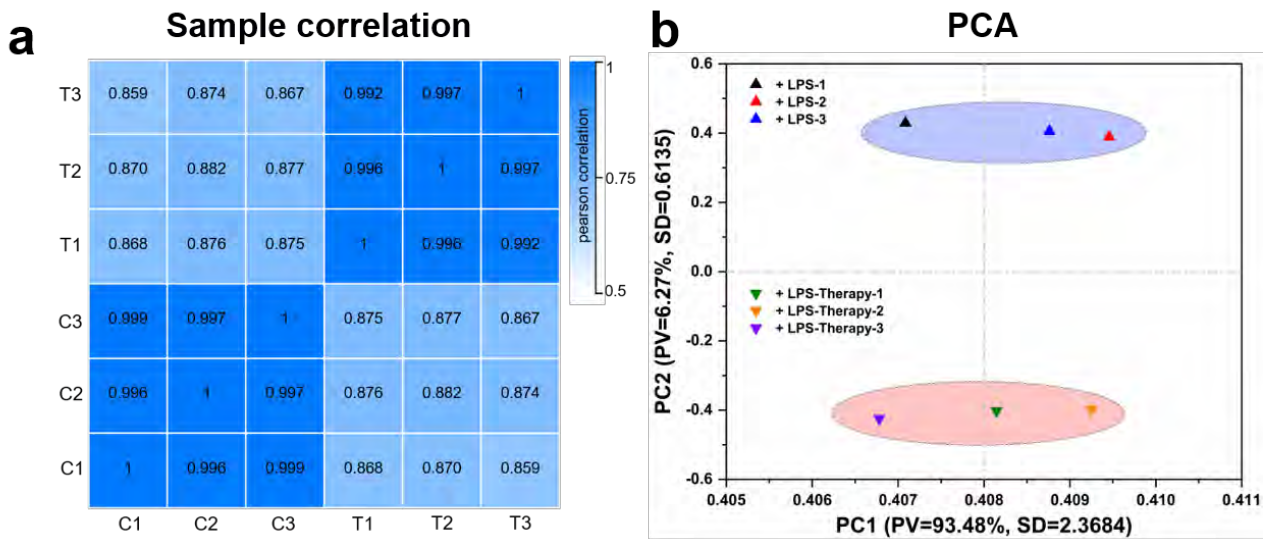

Fig. S14. (a) Pearson correlation coefficient analysis and (b) principal component analysis of the RNA sequencing samples between the two groups.

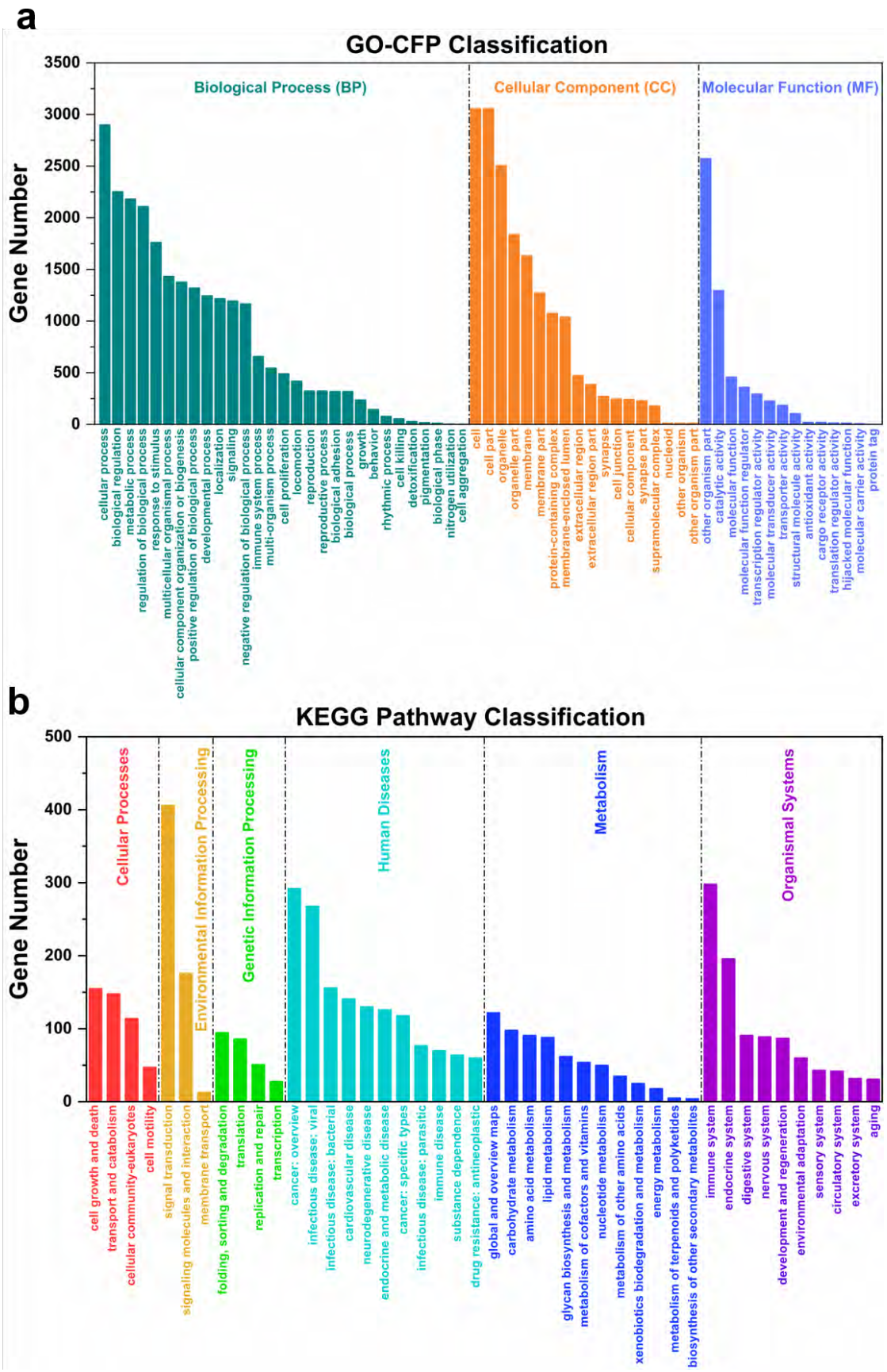

Fig. S15. (a) Gene ontology (GO) classification and (b) Kyoto Encyclopedia of Genes and Genomes (KEGG) pathway classification among differentially expressed genes (DEGs) of macrophages.

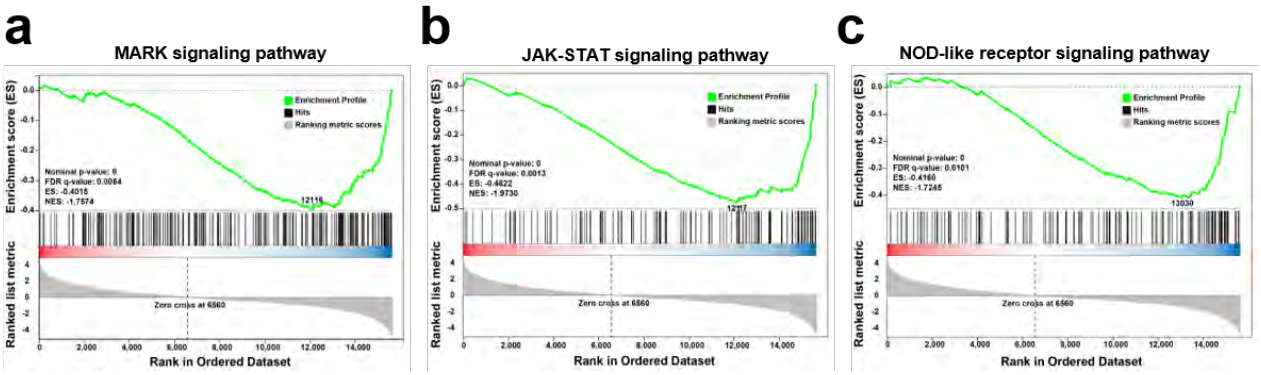

Fig. S16. Gene set enrichment analysis (GSEA) results of (a) MARK signaling pathway, (b) JAK-STAT signaling pathway and (c) NOD-like receptor signaling pathway.

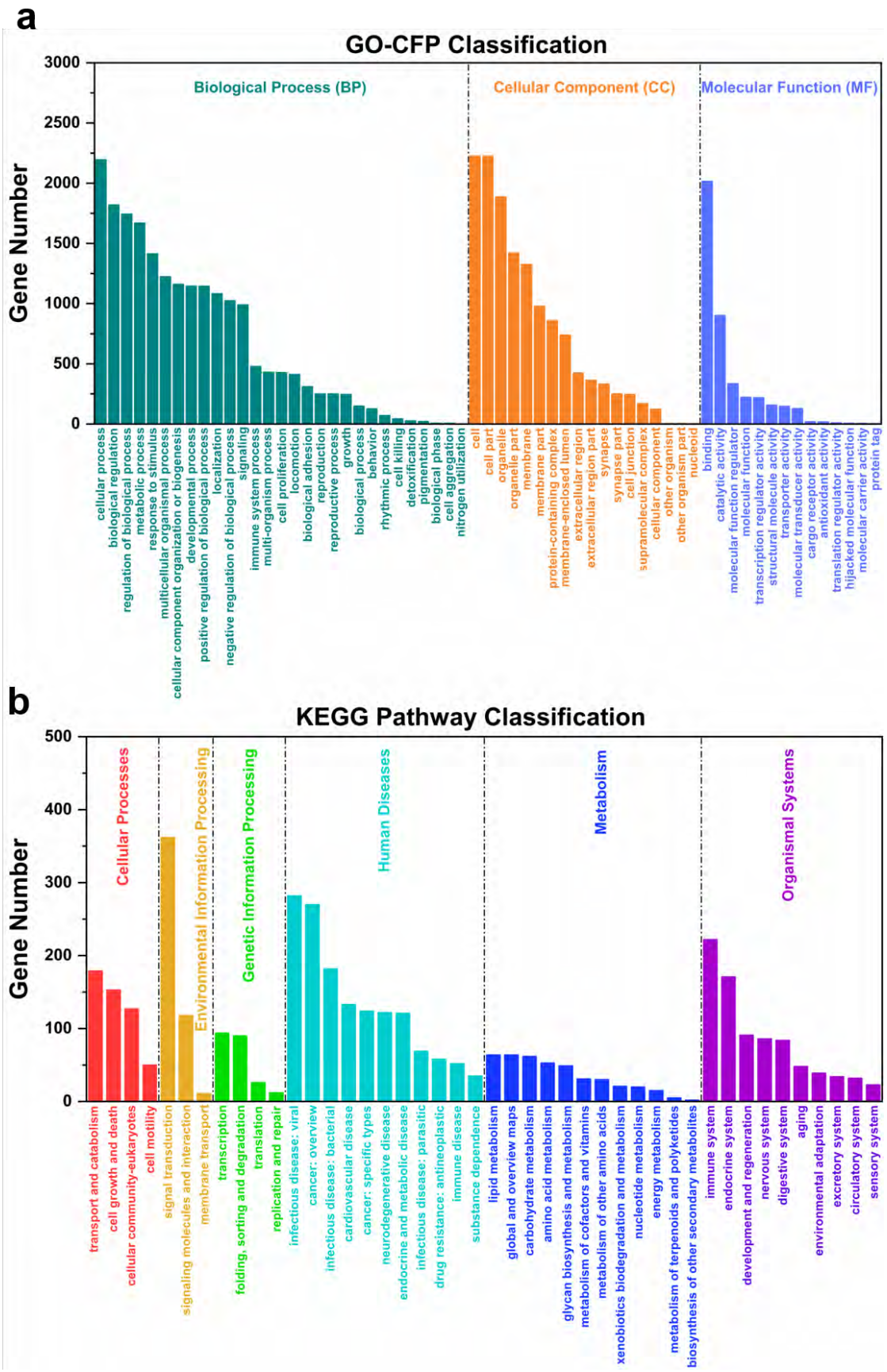

Fig. S17. (a) GO classification and (b) KEGG pathway classification among DEGs of chondrocytes after conditioned culture.

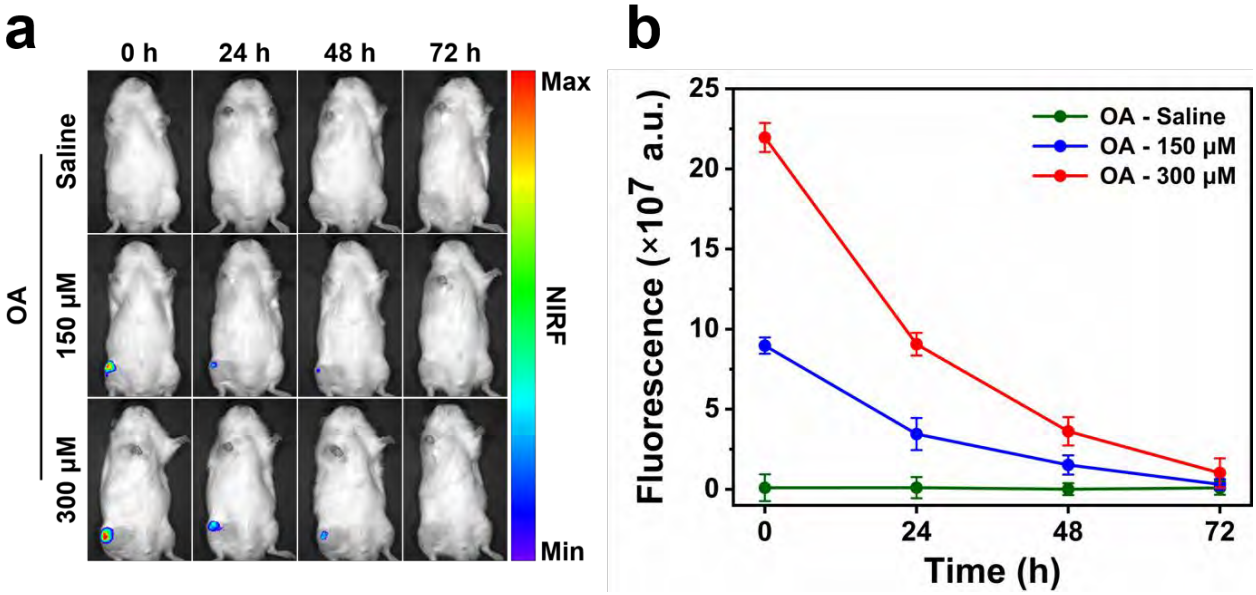

Fig. S18. Retention in the articular cavity of $Fe_3(CO)_{12}$@Croc-PEG5K. (a) NIRF images of rats at different time points after intra-articular injection and (b) Corresponding $NIRF_{820}$ intensity of (a).

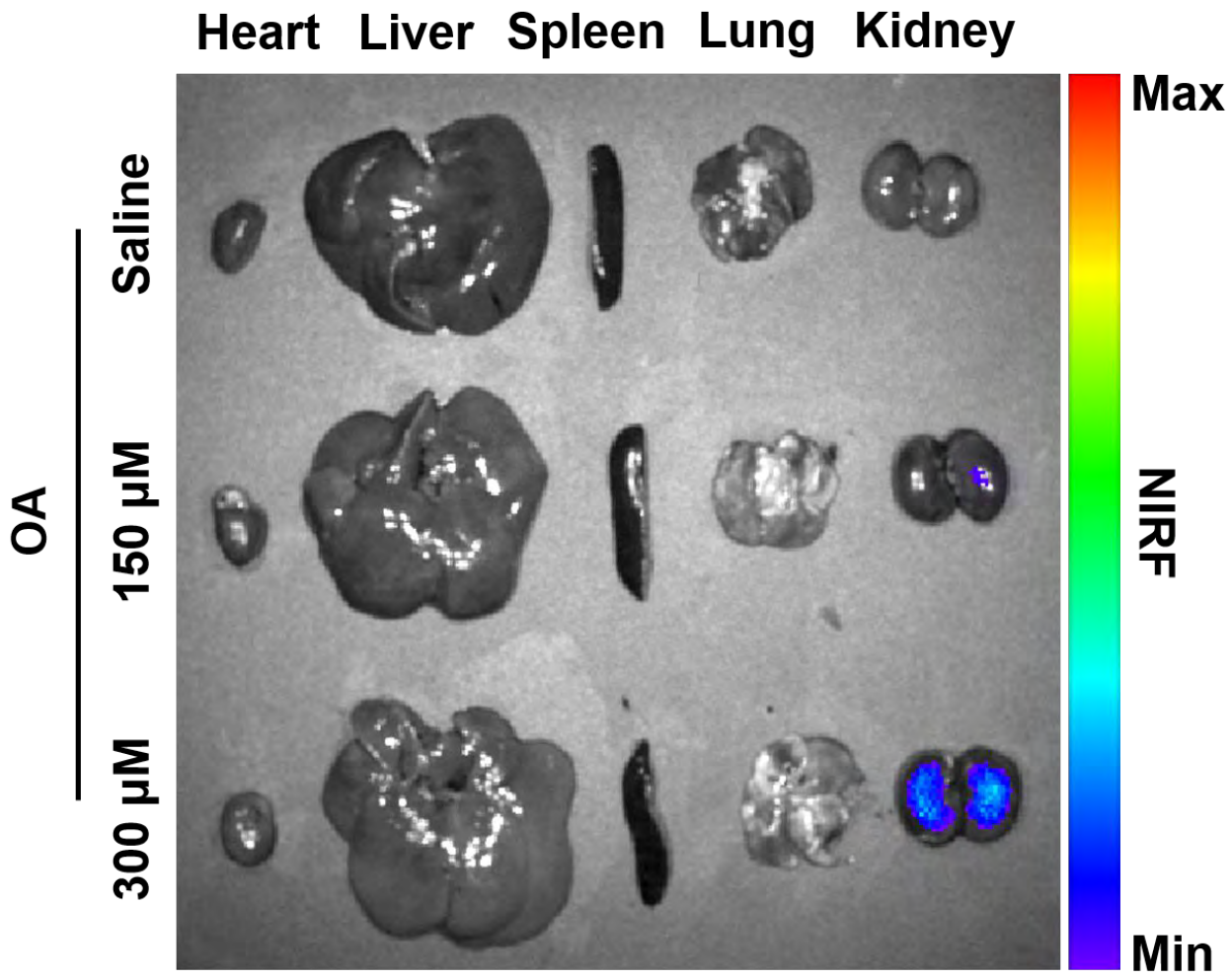

Fig. S19. Biodistributions of $Fe_3(CO)_{12}$@Croc-PEG5K in the major organs of rats at 72 h after intra-articular injection.

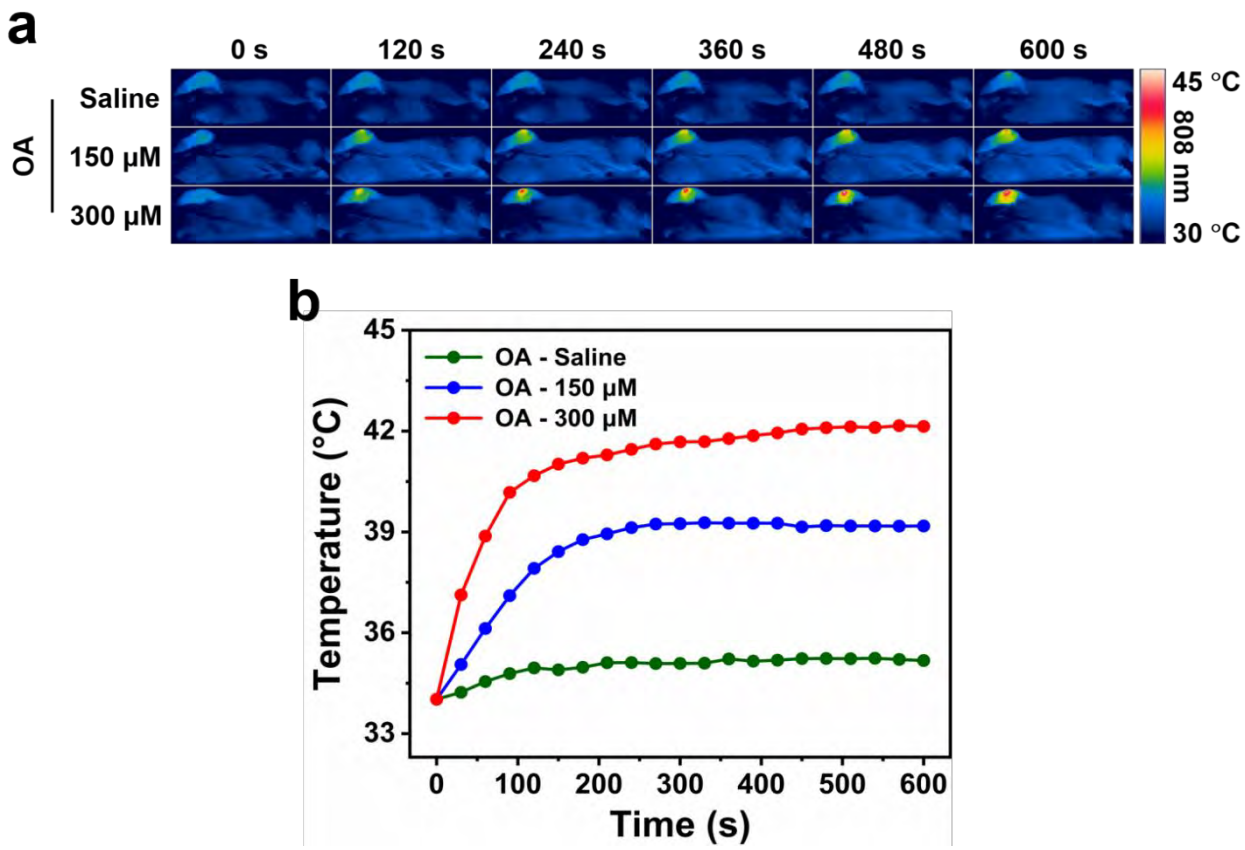

Fig. S20. *In vivo* photothermal effects of $Fe_3(CO)_{12}$@Croc-PEG5K. (a) Thermal images and (b) Temperature at different time points (0 ~ 10 min) under NIR laser irradiation (1.0 W/cm^2).

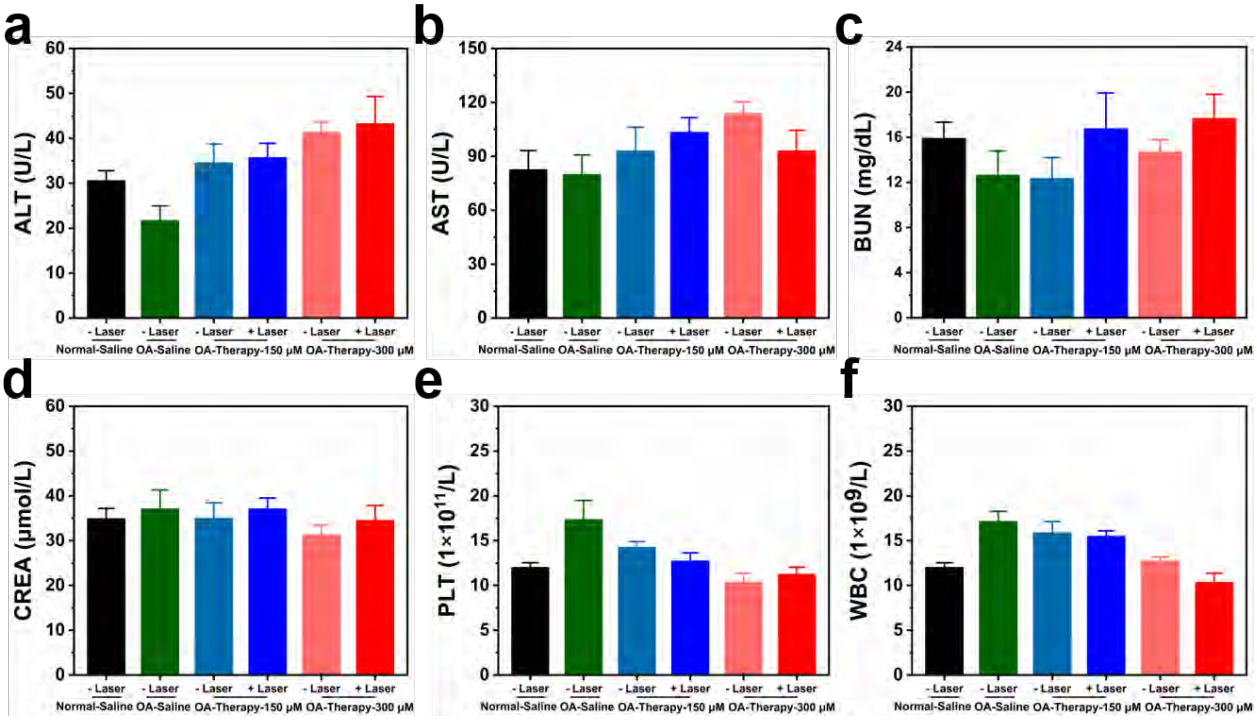

Fig. S21. Biochemical and blood routine assessment of rats after different treatments. (a) Alanine transaminase (ALT), (b) Aspartate Transaminase (AST), (c) Blood urea nitrogen (BUN), (d) Creatinine (CREA), (e) Platelet (PLT) and (f) White blood cell (WBC) analysis.

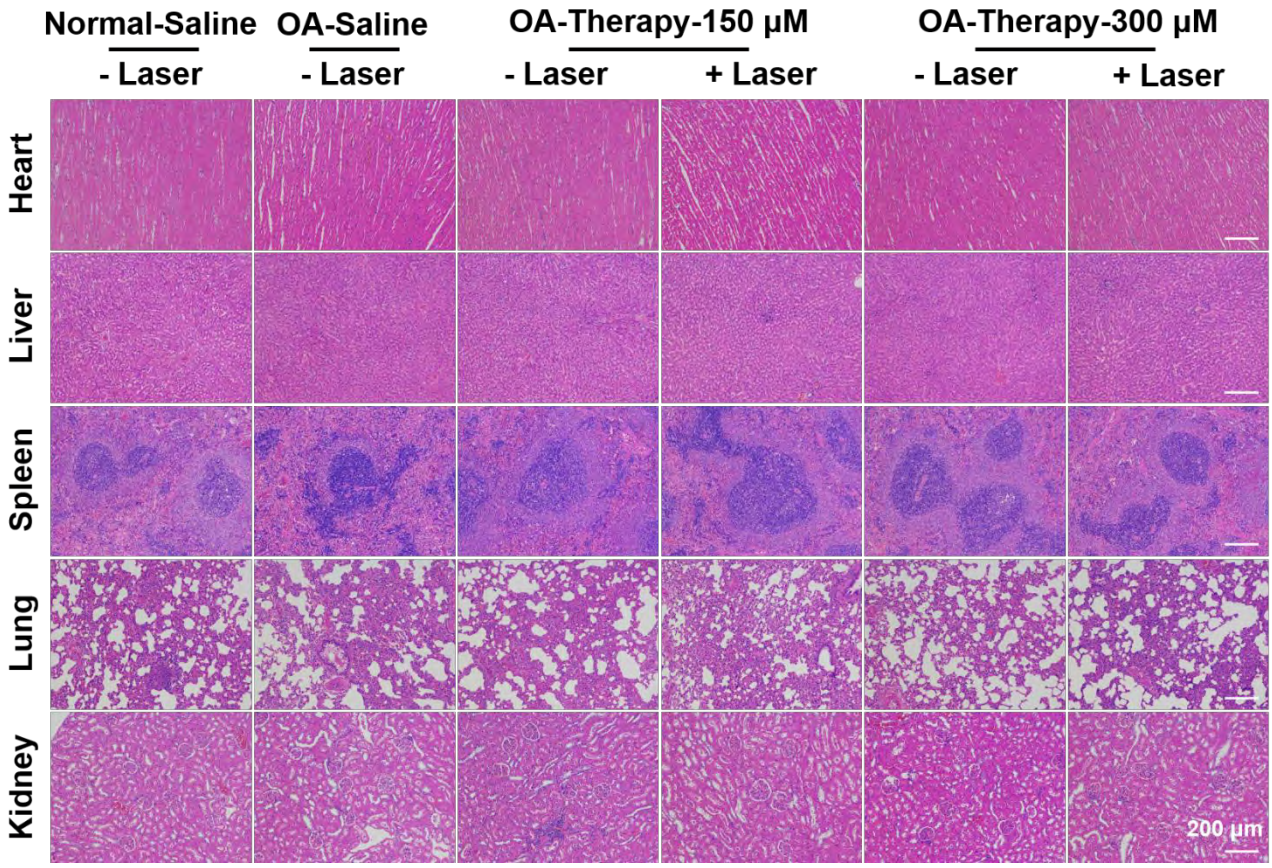

Fig. S22. Hematoxylin-eosin (HE) staining of the heart, liver, spleen, lung and kidney of rats after different treatments.

Table S1. Primer sequences used for qPCR.

Genes	Forward primers	Reverse primers
IL-1β	GAAATGCCACCTTTTGACAGTG	TGGATGCTCTCATCAGGACAG
IL-6	TCTATACCACTTCACAAGTCGGA	GAATTGCCATTGCACAACTCTTT
TNF-α	CAGGCGGTGCCTATGTCTC	CGATCACCCCGAAGTTCAGTAG
iNOS	GTTCTCAGCCCAACAATACAAGA	GTGGACGGGTCGATGTCAC
IL-4	ATGGATGTGCCAAACGTCCT	AAGCCCGAAAGAGTCTCTGC
CD206	AGACGAAATCCCTGCTACTG	CACCCATTCGAAGGCATTC
TGF-β2	CTTCGACGTGACAGACGCT	GCAGGGGCAGTGTAAACTTATT
IGF-1	CACATCATGTCGTCTTCACACC	GGAAGCAACACTCATCCACAATG
Col2a1	TGGTGCTCGGGGTAACGAT	GGCTCCAGGAATACCATCAGT
Acan	ATTTCCACACGCTACACCCTG	TGGATGGGGTATCTGACTGTC
Caspase3	CTCGCTCTGGTACGGATGTG	TCCCATAAATGACCCCTTCATCA
Bax	AGACAGGGGCCTTTTTGCTAC	AATTCGCCGGAGACACTCG